YAŞAR UNIVERSITY

GRADUATE SCHOOL

MASTER THESIS

A FRAMEWORK FOR CAPACITY EXPANSION PLANNING IN FAILURE-PRONE FLOW-NETWORKS VIA SYSTEMIC RISK ANALYSIS

NAZLI KARATAŞ AYGÜN

THESIS ADVISOR: ASSIST. PROF. DR. ÖNDER BULUT
CO-ADVISOR: ASSIST. PROF. DR. EMRAH BIYIK

DEPARTMENT OF INDUSTRIAL ENGINEERING

PRESENTATION DATE: 14.08.2020

BORNOVA / İZMİR
AUGUST 2020

We certify that, as the jury, we have read this thesis and that in our opinion it is fully adequate, in scope and in quality, as a thesis for the degree of Master of Science.

Jury Members: **Signature:**

Assist. Prof. Önder Bulut
Yaşar University

Assist. Prof. Emrah Bıyık
Yaşar University
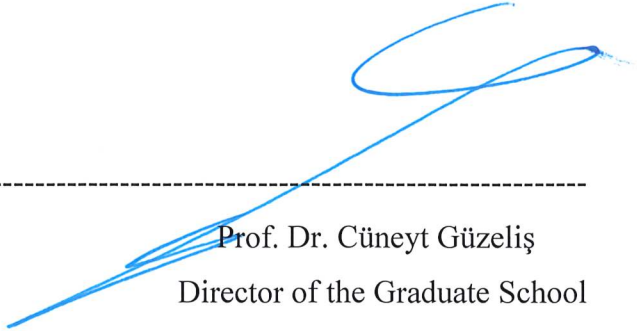
Assoc. Prof. Engin Karatepe
Dokuz Eylül University

Assoc. Prof. Ayhan Özgür Toy
Yaşar University

Assist. Prof. Özgür Kabadurmuş
Yaşar University

Prof. Dr. Cüneyt Güzeliş
Director of the Graduate School

ABSTRACT

A FRAMEWORK FOR CAPACITY EXPANSION PLANNING IN FAILURE-PRONE FLOW-NETWORKS VIA SYSTEMIC RISK ANALYSIS

Karataş Aygün, Nazlı

MSc, Industrial Engineering

Advisor: Assist. Prof. Dr. Önder Bulut

Co-Advisor: Assist. Prof. Dr. Emrah Bıyık

August, 2020

We propose a capacity expansion framework to guarantee a certain service level in failure-prone flow-networks composed of supply, demand and intermediate nodes, and arcs in between. We formulate the problem as a general stochastic optimization model to minimize the total cost of additional edge capacities. Our model allows considering different cost structures corresponding to the nature of different real-life applications. We consider a non-linear cost structure that captures both the immediate cost of investment and the cost of future risk. The feasible region is composed of the additional edge capacities that satisfies a probabilistic constraint (certain service level) which is the probability of total demand-not-satisfied is greater than a predetermined level is less than a risk threshold and a boundary constraint which is the additional edge capacities are greater than or equal to 0. These constraints are based on a systemic risk measure. Systemic risk measure, in contrast to traditional risk analysis on the component level, captures a holistic view of the system-wide operation and calculates the risk of unsatisfied demand. The requirement for system-wide analysis arises from the complex and nonlinear relationship between components of the system. Systemic risk is due to initial edge failures and the cascade of these failures throughout the system. Due to the stochastic nature of initial failures and certain supply and demand nodes, the distribution of unsatisfied demand is calculated via simulations embodied within a Grid Search Algorithm that identifies the feasible region. Cost-optimal edge capacity expansion is computed by a population-based heuristic optimization algorithm, namely, Differential Evolution. Our methodology can be applied to numerous fields including financial systems, power systems and supply chains. We

apply our proposed framework to a medium-size general flow-network, and conduct a comprehensive numerical study to investigate the effects of system parameters on the feasible region and optimal solution.

ÖZ

KOPMALARA EĞİLİMLİ AKIŞ AĞLARINDA SİSTEMİK RİSK ANALİZİ İLE BİR KAPASİTE ARTIŞ PLANLAMA ÇERÇEVESİ

Karataş Aygün, Nazlı

Yüksek Lisans, Endüstri Mühendisliği

Danışman: Dr. Öğr. Üyesi Önder Bulut

Yardımcı Danışman: Dr. Öğr. Üyesi Emrah Bıyık

Ağustos, 2020

Bu tezde, arz, talep ve aktarma düğümleri ile aralarındaki kenarlardan oluşan kopmalara eğilimli akış ağlarında, belirli bir hizmet seviyesini garanti etmek için bir kapasite artış plan çerçevesi öneriyoruz. Problemin amacı, en düşük maliyetli kapasite artış planlamasını bulmaktır ve problem genel bir rassal optimizasyon modeli olarak formüle edilmiştir. Modelimiz yapı itibariyle, çeşitli gerçek hayat uygulamalarına uyum sağlayan maliyet fonksiyonlarına izin vermektedir. Bu çalışmada kullandığımız maliyet fonksiyonu, direk maliyet ve gelecek risk maliyetlerini birlikte düşünür ve doğrusal olmayan bir yapıya sahiptir. Problemin olurlu bölgesi, karşılanmayan toplam talebin belirli bir seviyenin üstüne çıkma olasılığının belirlenmiş bir risk sınırından küçük olması ile tanımlanmıştır. Bu kısıtın bağlı olduğu sistemik risk ölçütü, sistem bileşeni özelindeki geleneksel risk ölçütü yerine, sistemsel operasyonlara bütüncül bir bakış açısı sağlar ve karşılanamayan toplam talep riskini hesaplar. Bu tarz bir sistemsel analiz ihtiyacı, sistem elementleri arasındaki karmaşık ve doğrusal olmayan ilişkilerden doğmuştur. Sistemik risk, sistemlerdeki ilk kopmalar ve bu kopmaların sistem genelinde artarak ilerlemesinden kaynaklanmaktadır. Karşılanamayan talebin dağılımı, Izgara Üzerinde Arama Algoritması içinde yer alan ve başlangıçtaki kopmaların, arz ve talep miktarlarının rassal doğası kullanılan simülasyonlarla hesaplanmıştır. En düşük maliyetli kapasite artışı ise, bir sürü tabanlı sezgisel algoritma olan Diferansiyel Evrim Algoritması kullanılarak hesaplanmıştır. Bu çalışmada sunduğumuz metodoloji, finansal sistemler, elektrik ağ sistemleri ve tedarik zincirleri gibi çeşitli alanlara uygulanabilir. Yaklaşımımızı orta büyüklükte genel bir akış ağına uyguladık. Buna ilaveten, sistem parametrelerinin olurlu bölge ve en düşük

maliyetli optimal çözüm üzerindeki etkilerini araştırmak için kapsamlı bir sayısal çalışma yürüttük.

Anahtar Kelimeler: Sistemik risk, peş peşe ilerleyen arızalar, akış ağı, diferansiyel evrim algoritması, rassal programlama, ızgara üzerinde arama algoritması.

ACKNOWLEDGEMENTS

First of all, I am thankful to my advisors, Assist. Prof. Önder Bulut and Assist. Prof. Emrah Bıyık, for their support, advices, valuable and important comments and suggestions. Their guidance helped me in all the time of research and writing of this thesis.

I want to express my gratitude and sincere thanks to my family. I would like to thank to my mother-in-law, Mukaddes Özdoğan for her persistent supports during this journey. I thank to my beloved sister, Nagihan Aygün for all her encouragements and supports. I would like to thank my dad and mom, Ayhan Karataş and Dilek Karataş, for always being my side and their endless support. I dedicated this thesis to my mom. I especially thank my one and only Abdullah Aygün for being a dream partner.

Finally, I would like to thank the entire Department of Industrial Engineering at the Yaşar University.

<div align="right">

Nazlı Karataş Aygün

İzmir, 2020

</div>

TEXT OF OATH

I declare and honestly confirm that my study, titled "A FRAMEWORK FOR CAPACITY EXPANSION PLANNING IN FAILURE-PRONE FLOW-NETWORKS VIA SYSTEMIC RISK ANALYSIS" and presented as a Master's Thesis, has been written without applying to any assistance inconsistent with scientific ethics and traditions. I declare, to the best of my knowledge and belief, that all content and ideas drawn directly or indirectly from external sources are indicated in the text and listed in the list of references.

Nazlı Karataş Aygün

Signature

………………………..

August 25, 2020

TABLE OF CONTENTS

LIST OF FIGURES

LIST OF TABLES

SYMBOLS AND ABBREVIATIONS

SYMBOLS:

$\mathcal{G}$	Network graph
$\mathcal{V}$	Set of Nodes
$\mathcal{E}$	Set of edges
$\mathcal{D}$	Set of demand nodes
$\mathcal{S}$	Set of supply nodes
$\mathcal{I}$	Set of intermediate nodes
$\mathcal{E}_D$	Set of demand edges
$\mathcal{E}_S$	Set of supply edges
$\mathcal{E}_I$	Set of intermediate edges
$\mathcal{E}_j$	Set of edges connected to node j
$\mathcal{E}_{IF}$	Set of initially failed edges
$\mathcal{X}$	Set of supply capacities, demand levels and edge capacities realizations
κ	Set of initial edge failures
Ω	Set of finite scenarios
Ω_r	Set of finite scenarios under which acceptability criterion is satisfied
N_i	Set of neighbors of edge i
$\mathcal{S}_R$	Set of supply nodes having random capacity
$\mathcal{D}_R$	Set of demand nodes having random capacity
i	Edge index
j	Node index
ω	Scenario index
L_j	Demand level of node $j \in \mathcal{D}$
$\bar{G}_j$	Capacity of supply generation node $j \in \mathcal{S}$

$\bar{P}_i$	Capacity of edge before investment $i \in \mathcal{E}$
Y_j	Unit cost of supply at node $j \in \mathcal{S}$
θ_j	Unit cost of unsatisfied demand at node $j \in \mathcal{D}$
β_i	Unit cost of flow on edge $i \in \mathcal{E}$
ρ_i	Unit cost of overload on edge $i \in \mathcal{E}$
c_i	Additional edge capacity for edge $i \in \mathcal{E}$
c	Additional edge capacity vector
v_{ij}	The direction of flow on edge $i \in \mathcal{E}_j$
g_j	Supply at node $j \in \mathcal{S}$
y_k	Fraction of satisfied demand at node $j \in \mathcal{D}$
p_i	Flow on edge $i \in \mathcal{E}$
s_i	Overload on edge $i \in \mathcal{E}$
$q(\omega)$	Probability of the particular scenario ω
$\Lambda(\mathcal{G}, \mathcal{X}, \kappa, c)$	Aggregation function
$\mathcal{A}$	Acceptance set
$R(\mathcal{G}, \mathcal{X}, \kappa)$	Systemic risk measure
ξ	DNS threshold
α	Risk threshold
$\eta(c)$	Capacity expansion cost function
k_1, k_2	Unit cost of additional capacity for Group-1 and Group-2, respectively
k_3	Cost of future risk
Q_1, Q_2 respectively	Fixed cost of additional edge capacity for Group-1 and Group-2,
T	Time until probabilistic constraint is not satisfied
Θ	Time until the next capacity expansion study
$\lambda(c_1, c_2)$	Parameter of the distribution of T

N	Size of the population
n	Problem dimension
g	Generation index
g_{max}	The maximum number of generations
x_g^j	j^{th} target individual at generation g
v_g^j	j^{th} mutant individual at generation g
u_g^j	j^{th} trial individual at generation g
F	Scaling factor
CR	Cross-over rate
$f(\cdot)$	Fitness function
ur_i	Utilization rate of edge i
A	Edge-edge adjacency matrix
λ_D	Dominant eigenvalue of A
ζ_D	Eigenvector related to λ_D
μ_j	Mean of the supply generation or demand level
σ_j	Standard deviation of the supply generation or demand level

ABBREVIATIONS:

DNS	Total Demand-Not-Satisfied
GSA	Grid Search Algorithm
DE	Differential Evolution
FP	Flow-Network Optimization Model
TI	Test Instance

CHAPTER 1

INTRODUCTION

Modern societies depend highly on the proper functioning of many systems with multiple components, structural and operational relations. Some examples of these complex connected systems are financial systems, power, supply chains and transportation systems. These systems, as being organized as large network structures, are open to various threats that may cause failures affecting numerous components. Due to the complex and nonlinear relationship between components of the complex networks, disruption of a component might trigger other failures in the system, and therefore cause a complete malfunction. In other words, an initial breakdown can even cause a complete system failure when it propagates with a cascading mechanism. Although they are not so frequent, such systemic failures result in a vast amount of direct and indirect costs to the firms and society. The networks are inherently open to this *large but rare* cascades that are triggered by a small initial failure. To mitigate or decrease the losses from such catastrophic failures, it is inevitable to analyze complex connected systems along with potential threats that may affect them. Hence, a requirement for the analysis of system-wide operations and underlying risk factors has emerged. In this direction, systemic risk studies gained importance and came into prominence in the existing literature. Unlike traditional risk on the element level, systemic risk deals with the probability of the system-wide failures that affects the entire system, and provide a holistic view to the system operations.

In this thesis, we propose a capacity expansion framework to guarantee a certain service level in general failure-prone flow-networks. We formulate the problem as a general stochastic optimization model, which is named as capacity expansion optimization model, to minimize the total cost of additional edge capacities. We consider a general flow-network with four types of elements: (i) supply (source) nodes that provide positive net flow to the system and have capacity limitations, (ii) demand nodes that have negative net flow as being a consumption point (iii) intermediate nodes (transmission) nodes have zero net flow that satisfies conservation rule where inflow

and outflow are equal, (iv) capacitated edges that allow flow between these nodes. In our network structure, we consider the stochastic nature of supply and demand levels to better mimic real-life environments. Moreover, we assume that total supply generation capacity is greater than or equal to total demand level for a well-defined problem. The capacitated edges are considered as failure-prone, and intolerant to overload. Under the nominal conditions, the system is capable to satisfy the total demand (no unsatisfied demand) and there is no requirement for extra edge capacity. However, in the presence of cascading mechanism, an initial edge failure might trigger other failures in the system, and hence, result in unsatisfied demand. We formulate a flow-network optimization model to calculate flow and overload on the edges and unsatisfied demand. Our flow-network optimization model is a generic model that consists of four cost components that are cost of supply, cost of flow on edges, cost of overload on edges and cost of unsatisfied demand. Hence, it can be adapted to solve different-real life applications by tuning the model parameters.

The edge capacities that guarantee a certain service level, namely, admissible edge capacities, are defined by a probabilistic and a boundary constraint that are structured using a systemic risk measure. To build these constraints, we benefit from pioneering work of the Chen et (2013) and Feinstein et al. (2017) on systemic risk measures which are formulated using two elements: (i) *aggregation function* is a system-level performance metric that provides a random outcome based on the system performance, (ii) *acceptability criterion* checks whether the distribution of random outcome satisfies a certain acceptance definition. In this study, we consider the probability of total demand-not-satisfied (DNS) that is greater than a predetermined threshold as a system-level performance indicator. DNS is obtained by solving flow-network optimization model for instance of supply, demand and initial edge failures. The distribution of DNS is calculated from the solution of flow-network optimization model for all instances (scenarios) of supply, demand and initial edge failures. *Acceptability* is defined by the probability of DNS that is greater than a predetermined level is less than a threshold. Hence, admissible edge capacities (feasible region) are described as follows: the set of additional edge capacities that satisfies *acceptability*. We compute the admissible edge capacities via a grid search algorithm (GSA) that approximates the boundary of the feasible region. Since aggregation function is monotone in nature, computing the boundary of the feasible region is sufficient to define the whole feasible

region. GSA works on a grid defined *a priori* where every grid point is considered as a candidate additional edge capacity. The algorithm moves on the grid by evaluating grid points according to acceptability criterion. Each evaluation requires Monte-Carlo simulation such that, given edge capacities (given a grid point), the distribution of DNS is calculated using scenarios generated by random supply, demand and initial failures.

The cost-optimal capacity expansion is computed via a population-based heuristic optimization algorithm, namely, differential evolution (DE). In our problem, the initial population for DE is obtained from the feasible region, and the fitness function of DE (cost function) is simply the objective function of the capacity expansion optimization model. Our model allows decision-makers to consider different cost structures (linear or non-linear) corresponding to the nature and operational strategies of different systems.

Our methodology can be applied to numerous fields including financial systems, power systems and supply chains. We perform a series of numerical experiments on the flow-network, to test our solution approach and understand the effects of system parameters on decisions and their cost.

The related literature is reviewed in Chapter 2. In this chapter, we introduce the studies that provide the followings: (i) the concept of systemic risk together with mitigation strategies in several areas such as finance, power systems and transportation networks, (ii) analysis of cascading failures and propagation mechanisms without working on mitigation strategies., (iii) systemic risk measure modeling approach that we benefit in this thesis. Moreover, we discuss the contribution of our study to the state-of-the-art in the literature.

In Chapter 3, we define our problem and introduce the features of our problem. We detail our approach to characterize system the system features that random supply, demand and initial edge failures. Moreover, we detail the methods that are employed for edge grouping.

Chapter 4 gives the details of our modeling framework for capacity expansion problem. In this chapter, we formulate flow-network optimization model, systemic risk measure and capacity expansion optimization model, and explain the relation between these models.

In Chapter 5, a flowchart of our solution approach is presented along with the details of the solution framework. Thereafter, grid search algorithm and differential evolution are explained in detail in Chapter 5.1. and 5.2., respectively.

Next, numerical study and discussions based on the findings are presented in Chapter 6. This chapter is divided into two subchapters: (i) the values of system parameters and test instances for numerical studies, (ii) results that we discuss the effect of parameter changes on feasible region and hence, cost-optimal capacity expansion.

Finally, a brief summary of the thesis and concluding remarks are presented in Chapter 7. Moreover, future research directions are also discussed in this chapter.

CHAPTER 2
LITERATURE REVIEW

In contrast to traditional risk analysis on the component level, systemic risk analysis provides a holistic view of the system-wide operation and underlying risk factors (Lucas et al., 2018), and has supplanted traditional risk on the element level (Ledwoch et al., 2016). It corresponds to the risk or probability of breakdowns in an entire system, as opposed to breakdowns in individual parts or components, and reveals the interplay between system components (Kaufman & Scott, 2003). Systemic risk is due to *shocks* and *propagation mechanisms*: *shocks* are the component failures; *propagation mechanisms* are the cascade of these failures due to complex connections between the components of a system (Bandt & Hartmann, 2000).

Financial crisis in 2007-2009 revealed the analysis of risk at firm-level is not sufficient to capture the breakdown probability of an entire system (Chen et al, 2013). During this crisis, shocks at few companies propagated and brought down the entire financial system and real economy, and then, the regulations and measurements of systemic risk has gained importance in economy and financial market (Bullard et al., 2009). Similarly, Italian Blackout in 2003 (Buldyrev et al., 2010) and Northeast Blackout in 2003 (Cassidy et al., 2016) showed that complex connected systems are prone to failure that can be caused by a random local event or malicious attacks. Consequently, risk quantification in power networks has gained attention of the researchers. Due to the tsunami in Japan on 11 March 2011, area that host the many advanced technology manufacturing firms is destroyed, and it causes a major impact on their supply. Hence, various manufacturing companies from all over the world, and supply chains are affected and their production is disrupted (Olson & Swenseth, 2014). In fact, globalization in supply chain increased vulnerability to disruptions like natural disasters and terrorism (Kleindorfer & Saad, 2005). As a result, system-wide risk assessment in supply chain management has gained importance (Stecke & Kumar, 2009).

Systemic risk is mainly applied to finance and economics in the literature. The study of Eisenberg and Noe (2001) is a pioneering work for integration of the rich network structures in the systemic risk models. In their study, contagion of linkages due to interbank liabilities is studied and a linear programming problem that gives the solutions for clearing payment vector is formulated. The domino effect due to a single bank breakdown base on the interbank relationships in German banking system is studied by Upper and Worms (2002). Boss et al. (2006), presented a model called Systemic Risk Monitor (SRM) to assess the systemic risk in the Austrian banking system. Cont et al. (2010), developed a quantitative methodology to analyze the potential contagion in interbank networks. They apply their model on Brazilian financial system. Capponi and Chen (2015), used the idea of Eisenberg and Noe (2001) to develop a multi-period systemic risk mitigation strategy and built a controlled clearing-payment system.

Systemic risks related to nature, technology and social systems is a macroscopic phenomenon resulting from elements' micro-level relations in a complex system with each other and their environment (Lucas et al., 2018). Although systemic risk has increased its prominence in finance literature, it is applicable to diverse areas such as power systems (Fang et al., 2014; Cassidy et al., 2016), supply chains (Ghadge et al., 2013; Ledwoch et el., 2016), transportation networks (Zhao et al, 2015; Pitilakis et al., 2016); water networks (Distefano et al., 2018). The aforementioned studies in this paragraph and some other exemplary studies are introduced throughout this chapter.

Baldick et al. (2008) claims that power systems, which are engineered designs, are operated to mitigate the risk of complete failures, hence it is unlikely that single element failures result in cascading failures. On the other hand, they emphasize that multiple elements' failures or operational mistakes might occur and trigger chains of failures. Fang et al. (2014) provide a comparison between network-centric and power flow models for edge capacity allocation in a power system via a systemic view. They formulate a multi-objective optimization problem with two conflicting objectives: maximizing resilience and minimizing a linear investment cost. In the study of Cassidy et al. (2016) the use of systemic risk measures from the finance literature is proposed to calculate the cascading failure risk in power grids, and plan capacity expansion.

Oehmen et al. (2010) discuss that system-oriented supply chain risk management is a shortcoming of the existing literature, and it's important to identify supply-chain risks

from a system perspective due to volatility in global sales and supply markets. Ghadge et al. (2013) also emphasize from another perspective that systems thinking based approaches are not well developed in the supply chain risk management literature. To fill this gap, they propose a holistic, systematic and quantitative risk assessment framework for measuring the overall risk behavior in supply chain. Pointing out the gap in the literature, system approach to the supply chain risk management has gained importance during the last decade. Especially, the studies that work on the supply chain disruptions, propagation mechanisms and resilience has been attracting researchers as follows: Behdani et al. (2012) proposed a framework that integrates pre-disruption and post-disruption perspectives that point out risk identification and risk treatment, and disruption impacts, respectively. They also provide a detailed literature review on the disruption phenomena, and introduce the risk quantification methods in detail. They classified the methods as follows: (i) qualitative/semi-qualitative methods that are analytic hierarchy process (AHP), expert group training, expert opinion (survey) and failure mode and effect analysis (FMEA), (ii) quantitative/semi-quantitative which are Petri-net, system dynamics, graph theory, discrete event simulation, input-output modeling. Scheibe and Blackhurst (2017), work on a qualitative research project to analyze the disruption propagation mechanisms throughout multiple tiers in the supply chain. For application of their approach, they work on a seven three-tiered supply chains where each tried consists of a focal firm, a supplier to the focal firm and a customer of the focal firm.

The studies that analyze supply chain resilience in the presence of disruption are as follows: Schmitt and Singh (2012) analyze inventory placement and back-up methodologies in a multi-echelon network and observe their effect on reducing supply chain risk from a holistic perspective. They employ fill-rate as a system performance indicator. Li and Zobel (2020) present a framework to investigate the supply chain network resilience in case of a disruption propagation that affects the whole system. To quantify the system resilience, they select three different network-level performance metrics: (i) number of healthy nodes that is total number of non-disrupted nodes in the presence of disruption propagation, (ii) the largest connected component is the largest connected subnetwork at a certain time after disruption, (iii) the ratio of largest connected subnetwork and average shortest path between any pair of nodes. Baghersad and Zobel (2020) propose a methodology based on the system resilience to

quantify the impact of supply chain disruptions on firms' performance. To measure the impact of disruptions, they use the followings: (i) operating performance measures that are change in operating income, change in return on sales, change in return on assets, change in sales, change in total assets, change in total costs and change in total inventory, (ii) stock prices.

There are studies in the supply chain literature that directly point out the systemic risk phenomena. Ledwoch et al. (2016) use 5 centrality metrics (eigenvector centrality, hub, authority, closeness, and betweenness) to assess systemic risk in supply chain networks, and set up an exemplary case study on the supply network of Honda Acura. Sun et al. (2017) study risk of oil supply from the systemic perspective of oil supply chain. They propose the use of four risk factors that are availability, accessibility, acceptability and affordability to quantify the systemic risk of oil supply.

Kamalahmadi and Parast (2017) provide an assessment of mitigation strategies against in a disruption in supply chain. They evaluate the impact of three mitigation strategies: prepositioning inventory, backup suppliers, and protected suppliers on the results of the disruption impacts. Zhao et al. (2018) propose a decision support system to analyze the robustness of supply chain networks against disruptions using topological analysis and performance measurement relevant to a supply chain context. They also present an optimization model that aims increase the performance of supply network. Their framework allows measurement of the performance of a supply chain network in the presence of a disruption, and understanding vulnerabilities of the network before a disruption. They employ four metrics to test the supply chain performance: the size of the largest functional subnetwork, average supply path length, total units delivered from supply to demand and average delivery cost.

Zhao et al. (2015) present a model for cascading failures that consider dynamic redistribution of flow in the networks, and study robustness of different network topologies. They apply their framework the interconnected traffic networks of Beijing city. Pitilakis et al. (2016) propose an integrated framework for the probabilistic systemic vulnerability and risk assessment of transportation and utility networks. Their methodology is demonstrated through case studies in the road network and the harbor of Thessaloniki city. Salomon et al. (2020) utilize from resilience metrics to quantify the systemic risk in general complex systems. The applicability of their proposed approach is demonstrated on Berlin's U-Bahn and S-Bahn systems and a multi-stage

axial compressor. Distefano et al. (2018) present a study that combines the structural decomposition analysis with network measures of systematic vulnerability to exogenous supply-shocks. With the help of network approach, they analyze the systemic structure and the evolution of the network in terms of potential vulnerabilities and allocation of a resources.

Another stream of research in the related literature focuses on analysis of cascading failures and underlying mechanisms in complex networks without specifically addressing mitigation strategies or capacity expansion plans. Watts (2002), worked on the global cascades that are happen rarely but result in large disruptions on some random networks in his pioneering study. He presented a simple, binary-decision model which can be used to set up some explanations on the cascade mechanism in real systems. Crucitti et al. (2004) also studied *large but rare* failures resulted from a small initial disturbance. It is proven that if the initially failed node has the largest load in the system, the failure of this specific node results to total disruptions of the system. Buldyrev et al. (2010), presented a model to capture failure propagation on the interdependent network. They resulted that the vulnerability of interdependent networks to random failure increases with the increasing interdependence from the robustness perspective. Wynne and Dressel (2010) discussed the effect of bovine spongiform encephalopathy (BSE) not only on livestock and feed industries but also on the financial sector. Świerczek (2014) investigated the relationship between the level of supply chain integration and cascading failures. Even though high integration is promoted in traditional supply chain literature, over-dependence between partners/agents may result in "snowball effect" that amplifies the effect of disruptions. Korkali et al. (2017) studied several failure propagation mechanisms under different power and communication network structures. Zang and Moura (2017) focused on the question that where a small number of localized failures can lead to significant number of failures in the network. In their presented model, namely the Dynamic Bond Percolation (DBP) process, the failure probability of an edge depends on the number of failed neighboring edges in the network, and the recovery probability depends on the number of working neighboring edges. They applied their model on the 118-node IEEE test bus power grid. La (2017) developed a general model to capture the propagation of failures from one component to another both within the system and across multiple interdependent systems.

Systemic risk measure represented in this study is based on the pioneering work of Chen et al. (2013) and Feinstein et al. (2017). In the study of Chen et al. (2013), it is shown a variety of models can be obtained depending on the choice of aggregation function and base scalar risk model. Moreover, this study provides an explicit structural characterization of the systemic risk models. In the study of Feinstein et al. (2017), the systemic risk measure is constructed as a combination of two entities which are a value model or *aggregation function* and *acceptability criterion* which allows the simultaneous analysis of the entities in the financial system. In their study, *aggregation function* is defined as a value model which assigns capital allocation of the entities into a stochastic outcome; whereas *acceptability criterion* defines the subset of the random variables that are acceptable to the regulator of the system. The result of the model introduced in that study can be interpreted as the set of the additional allocation that is required to make the current system acceptable. Besides, they introduce a grid search algorithm to compute the systemic risk measures.

In this thesis, we use a systemic risk measure that benefits from the finance literature to find the admissible edge capacities that guarantee a certain service level. The systemic risk measure quantifies the system-wide risk, and provides a set of admissible edge capacities. Application of the financial systemic risk measures to the other networks is new to the literature. Three studies work such systemic risk measures: (i) Cassidy et al (2016), (ii) Eckert and Beer (2019), (iii) Salomon et al (2020). Cassidy et al (2016) use a systemic risk measure to find a set of acceptable component capacities under which the risk of power failure in the grid is acceptably low. They test their framework on the IEEE 118-Bus and 30-Bus systems, and simulate the cascading edge failures resulting from a set of initial edge failures. Their study is the first to apply financial systemic risk measures to another network. Eckert and Beer (2019) propose the use of financially inspired systemic risk framework in structural mechanics. Instead of simulating an initial failure and the resulting cascading failures they characterize the risk of an initial failure from the reliability perspective. Salomon et al. (2020) work on the use of financial risk measures to complex systems, such as turbines, industrial plants, and infrastructure networks using a resilience-based aggregation function. They apply their framework to a multistage axial compressor and U-Bahn and S-Bahn system of Berlin where their simulation is based on initial component failures and initial failures that might lead to cascading failures, respectively. In our study, we both

simulate initial failures and resulting cascading failures. Cassidy et al. (2016) and Salomon et al. (2020) assume randomness only for initial edge failures; however, in our study we also assume the network has random generations and demand levels. Cassidy et al. (2016), and Eckert and Beer (2019) assume linear cost function that provide solution on the boundary of the feasible region. On the other hand, we consider a nonlinear cost structure, and propose the use of population-based heuristic to handle general cost structures. In the studies of Cassidy et al. (2016) and Salomon et al. (2020), a grid search algorithm (Feinstein et al., 2017) is employed to compute the systemic measure. In our thesis, we also use grid search algorithm to calculate the feasible region. Since grid search algorithm requires Monte-Carlo simulations to evaluate each grid point, the computational complexity increase with the increase in the number of elements, which corresponds to the problem dimension, that are subjected to capacity expansion. Hence, the efficiency of the algorithm can be increased if the elements that are subjected to capacity expansion are subdivided into groups, and allocating same additional capacity to the members of the same groups. For this grouping purposes, Cassidy et al. (2016) divide the lines into two groups according to a centrality index that is calculated using the number of shortest paths that the line is on. Salomon et al. (2020), grouped the metro stations in U-Bahn and S-Bahn system of Berlin according to their node degree. Since, selecting a proper edge grouping method that is in line with the nature of real-life application is critical. In our study, we employ two methods for grouping purposes that are utilization-based and eigenvector centrality, and we observe their effect on the feasible region, and hence, optimal investment. The numerical experiment based on edge grouping method also differs our study from the previous works.

Compared to the state-of-the-art in the literature, contributions of this thesis are four-fold: (i) flexibility to handle general edge capacity expansion cost structures by employing a population-based heuristic, DE, for cost optimization problem, (ii) a generic flow-network model that considers cost of supply, cost of flow on edges, cost of overload on edges and cost of unsatisfied demand (a service level metric), (iii) taking into account the stochastic nature of both supply (i.e., renewables in power networks) and demand from the systemic risk perspective, (iv) use of eigenvector centrality for *edge* grouping (extending the common use for node grouping) in systemic risk measurement. These contributions, together with the systemic risk

approach, provide a unified framework for the analysis and design of flow-networks to achieve cost-optimal service improvement.

CHAPTER 3
PROBLEM DEFINITION

Our problem is defined as follows: finding cost-optimal capacity expansion that satisfies a certain service level in general failure-prone flow-networks. We first identify the set of additional edge capacities that need to be invested in (admissible edge capacities) such that the probability the total demand-not-satisfied (DNS) is within acceptable levels under shocks (i. e., edge failures). Then, we find the cost-optimal capacity expansion among admissible edge capacities.

In this thesis, we employ a medium-size flow-network represented by a $\mathcal{G} = (\mathcal{V}, \mathcal{E})$, where $\mathcal{V}$ and $\mathcal{E}$ denote the set of nodes and edges, respectively. The considered flow-network has random characteristics and open to initial edge failures. Specifically, we consider the stochastic nature of both supply (i.e., renewables in power networks) and demand for the random features of the network. In Chapter 3.1, we explain our modeling methodology and scenario generation approach to characterize randomness in supply generations and demand levels.

When the system is working under nominal conditions (no failure), there is neither over capacity requirement nor unsatisfied demand, i.e., DNS = 0. However, we consider a failure-prone flow-network where an initial failure might trigger other failures in the system, and hence, result in DNS. In Chapter 3.2., we introduce the details of our scenario generation approach based on edge failures and respective edge failure probability.

We compute the set of admissible edge capacities using grid search algorithm (GSA) that approximates the feasible region boundaries on a predetermined n dimensional grid where n is the number of decision variables. Checking if a candidate solution (grid point) is feasible or not, requires Monte-Carlo simulations as detailed in Chapter 5.1. Hence, its computational intensity is directly affected by the choice of n that is determined by the number of edges that are subjected to capacity expansion. To exploit GSA more efficiently, it is proposed to subdivide edges into groups according to their

similarities, and assign same additional capacity to the edges that are in the same group. In Chapter 3.3., we explain the grouping methods that we use in this study. In Monte-Carlo simulations we use scenarios generated by an instance of random supply, demand and initial edge failures.

An exemplary real-life infrastructure network that can be considered within the scope of our problem is power networks. In power networks, there are generator and load busses that corresponds to supply, demand and intermediate nodes in our network representation. In power systems, there might be random supply generation if renewable energy sources are employed. Moreover, there exist randomness in demand in power networks. Lines transmit power through the system, likewise edges transmit flow in our case. There might exist both single or multiple line failures in power systems. Some of the reasons of these type of failures are maintenance activities, natural disasters, terrorist attacks etc. These failures might result to removal (dysfunction) of the subjected link which changes the distribution of the power on the links. Consequently, the flow on some links might change and exceed its capacity (overload), and hence, may result to subsequent link failures, namely, cascading failures.

3.1. Random Supply and Demand

In our network structure, we consider the stochastic behavior of supply and demand which are used for scenario generation during Monte-Carlo simulation. The representation of a random variable is a design issue in stochastic problems. It is difficult or inconvenient to get samples from a continuous distribution for some instances, hence using a discrete representation is more convenient (Chakraborty, 2015). In order to generate finite number of scenarios to represent the stochastic nature of supply and demand, we employ discretized versions of the normal (*d-normal)* and uniform (*d-uniform)* distributions. We assume that random supply nodes are distributed *d-normal* with parameters (μ_j, σ_j) for random supply node j. On the other hand, random demand nodes j are distributed either *d-normal* (μ_j, σ_j) or *d-uniform.* We obtain *d-normal* (μ_j, σ_j) distribution as follows. We first let n_{int} be the number of equal length intervals over the range $[\mu_j - 2\sigma_j, \mu_j + 2\sigma_j]$. Then, we split the range into n_{int} bins, and use the corresponding $(n_{int} + 1)$ boundary points of the bins as scenarios. Each scenario corresponds to an instance for Monte-Carlo simulation. The

d-uniform distribution also uses the same range $([\mu_j - 2\sigma_j, \mu_j + 2\sigma_j])$, and same $n_{int} + 1$ boundary points, but this time the probabilities of the boundary points are equal.

As we increase n_{int}, we would be more capable of mimicking continuous distribution. On the other hand, total number of scenarios rapidly increases with the increased number of intervals. Hence, the trade-off between computation time and total number of scenarios must be taken into consideration while designing the numerical solution methodology.

3.2. Initial Edge Failures

Cascading failure is a sequence of dependent failures of individual components that successively weaken the system under consideration (Baldick et al., 2008). Our study, analyzes cascading edge failure mechanisms resulted from single or multiple edge failures. In the context of our study, a predetermined number of edges and their failure probabilities are defined. We employ two different methods to select a predetermined number of edges that are subjected to shocks, and are initially failed: (i) utilization-based, (ii) random.

In the utilization-based selection, the utilization rate ur_i of each edge i is calculated as follows:

$$ur_i = \frac{p_i}{\bar{P}_i} \in [0,1] \qquad (1)$$

where p_i is the flow on edge i and $\bar{P}_i$ is the capacity of edge i. Utilization rate of edge i is calculated under nominal conditions when there is neither additional edge capacity nor initial edge failure. Then, the predetermined number of edges with the largest ur_i are selected as the failing edges. In the random selection, however, initially failed edges are selected in a uniform random manner, and same certain probability is assigned to the edges that are initially failed.

Initial failure probabilities of the failed edges in utilization-based are determined in two ways. In the first one, failure probabilities are calculated based on the normalized utilization rates of the selected edges. Normalization is done in a way that total failure probabilities of the edges sum up to a certain value in $(0,1]$ that represents the real-life characteristics of systems under consideration. In the second one, failure probabilities

of the initially failed edges are assigned to a fixed common value. We assume that initial edge failures are independent, thus the probabilities of multiple edge failures are found by multiplication of the related single edge failure probabilities.

The utilization-based initially failed edge selection is prominent in the literature (Kinney et al., 2005; Cassidy et al., 2016). Intuitively, this method points out the targeted attacks or the most expected failures that start from the highest-load edges. On the other hand, random failures are likely to occur as a result of a natural event or a maintenance activity.

3.3. Edge Grouping

To reduce the computational complexity, we reduce the number of decision variables by dividing the edges into 2 groups. The same additional edge capacities are allocated to the members of the same group by which we can reduce the problem dimension, and solve it in a manageable time. This grouping idea is in line with the real-life applications and the existing literature (Cassidy et al., 2016; Feinstein et al., 2017, Salomon et al., 2020). For instance, Feinstein et al. (2017) exemplify subdivision of the nodes which are financial institutions based on their types such as banks, insurance companies etc. In Cassidy et al. (2016), the lines in a power grid are divided into two categories according to their centrality index.

We employ two different methods for grouping purposes: (i) utilization-based, (ii) eigenvector centrality. In utilization-based grouping, edges are assigned to groups based on their utilization rate ur_i (given in equation (1)). Then, edges with utilization rate above a predetermined threshold are assigned to Group-1, and the rest are assigned to Group-2.

The second method, eigenvector centrality measure provides a node criticality index that measures node importance based on the importance of its neighbors (Bonacich, 1972). We employ eigenvector centrality measure to obtain centrality index of the edges and use as grouping method as follows. For a given graph $\mathcal{G}$, we consider the edge-edge adjacency matrix $A = \{a_{ik}\}$ for edges i and k ($i, k \in \mathcal{E}$) such that $a_{ik} = 1$ if edges i and k are neighbors (connected to a common node), and 0 otherwise. Let N_i be the set neighbors of edge i, the centrality score of node i ζ_i is obtained as follows:

$$\zeta_i = \frac{1}{\lambda} \sum_{k \in N_i} \zeta_k = \frac{1}{\lambda} \sum_{k \in \mathcal{E}} a_{ik} \zeta_k. \quad (2)$$

16

Equation (21) can be rearranged as the eigenvector equation such that $A\zeta = \lambda\zeta$. To find non-negative ζ, the choice of is λ critical. Perron-Frobenius theorem (Gantmakher, 1959) states that dominant eigenvalue λ_D of A guarantees a unique and non-negative solution to ζ_D. The components of the related eigenvector ζ_D provides accessibility indices such that i^{th} component of ζ_D gives the centrality index of edge i. Similar to the utilization-based method, edges with eigenvector centrality index above a predetermined threshold are assigned to Group-1, and the rest are assigned to Group-2. An edge may have large number of neighbors but relatively low eigenvector centrality index if many of those neighbors have similarly low centrality indices. It can be regarded as a measure of how important an edge, based on the importance of its neighboring edges. To the best of our knowledge, such use of eigenvector centrality for *edge* grouping is new to the systemic risk literature.

In the next chapter, we explain our modeling framework based on our problem definition. Our modeling framework considers the problem features detailed in this chapter.

CHAPTER 4
MODELING APPROACH

Thus far, we defined our problem and the features of the problem. Throughout this chapter, we introduce our modeling approach and relations of the models that we use to build our cost-optimal capacity expansion framework. Our modeling framework starts with the flow-network optimization model (FP), that calculates the flow on the edges, overload on the edges and unsatisfied demand for a given edge capacity, an instance of supply, demand and an initial failure. If an initial failure triggers cascading failures, then (FP) is run repeatedly until system reaches steady-state (when there is no other failure), and DNS is calculated directly from at the steady-state. On the other hand, if there is no cascade, DNS is directly calculated from the first run of the (FP). To calculate DNS distribution, for a given additional edge capacity, which consists of the nonnegative elements, the same procedure is applied for all realizations (scenarios) of random supply, demand and initial edge failures. DNS distribution is used to check whether probabilistic constraint is satisfied for the candidate solution (additional edge capacity). Feasibility condition is set via a probabilistic constraint and a boundary constraint that is derived from a systemic risk measure. Since the members of candidate additional edge capacity are selected as nonnegative, boundary constraint is handled prior to the probabilistic constraint. Then, a candidate solution is said to be feasible, if the probability of DNS that is greater than a predetermined threshold is acceptably low, and the set of admissible edge capacities is updated accordingly. Otherwise, we discard this solution. After completing the probabilistic constraint check for every candidate solution, and finding the feasible region, we next, find the cost-optimal solution via capacity expansion optimization model. The illustration of the relation between the models are given in the following flowchart.
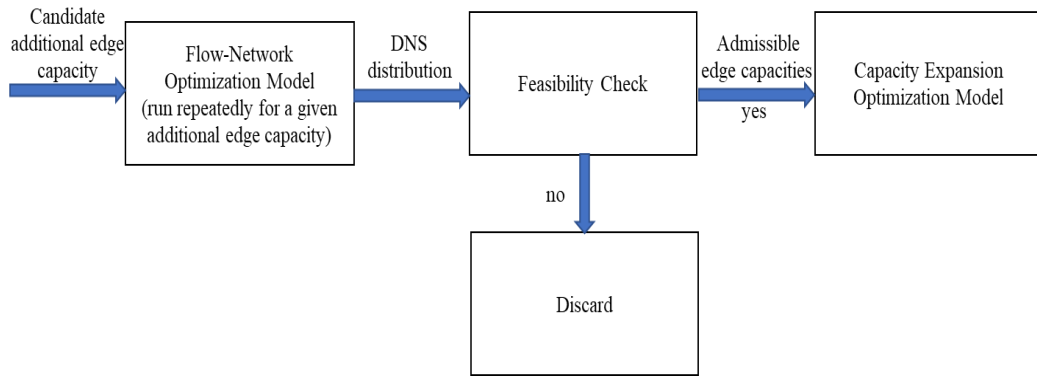
Figure 4.1. Flowchart of the Modeling Framework

The assumptions of our problem that we use to formulate flow-network optimization model, systemic risk measure and capacity expansion optimization model are as follows.

- Our problem is not modeled as a design problem such that framework introduced in this study works on a given network with certain characteristics.

- We assume that there exists randomness in supply and demand.

- Considered network is failure-prone where an initial failure might trigger other failures in the system.

- In this study, we consider edge failures only.

- To reduce the computational complexity, we divide edges into 2 groups such that the same additional edge capacities are allocated to the edges in the same group. As a result, the number of decision variables is reduced to 2.

- We assume that when the system is working under nominal conditions, i.e., neither initial failure nor additional capacity, there is neither over capacity requirement nor unsatisfied demand.

- Supply generation from the random supply node is assumed to be priceless. As we consider a system that fits to several real-life environments, we assume that random supply is priceless. As an example, in power networks, the cost of the supply from a renewable energy source can be considered as priceless. As a result of this assumption, system wants to utilize from all of the capacity of the random supply.

- For a well-defined flow-network problem, we assume total supply capacity is greater than or equal to total demand level.

In the following subchapters, we introduce the flow-network optimization model in Chapter 4.1., the systemic risk measure is explained in Chapter 4.2. and the capacity expansion optimization model is given in Chapter 4.3.

4.1. Flow-Network Optimization Model

We consider a general flow-network represented 66. The node set $\mathcal{V}$ is the union of demand $\mathcal{D}$, supply $\mathcal{S}$ and intermediate nodes $\mathcal{I}$ node sets. Capacitated supply (source) nodes provide positive net flow to the system. On the other hand, demand (sink) nodes have negative net flow as being consumption points, and intermediate (transmission) nodes, which have zero net flow, establish transfer between supply and demand nodes.

The edge set $\mathcal{E}$ is the union of demand edge $\mathcal{E}_D$, supply edge $\mathcal{E}_S$ and intermediate edge $\mathcal{E}_I$ sets and all of them are capacitated. Supply and demand edges are unidirectional, and maintain flow between supply and demand nodes and intermediate nodes. However, intermediate edges are bidirectional, and establish transfer between intermediate nodes.

In addition to the topological definition $\mathcal{G}$ of the network, we let $\mathcal{X}$ represent the stochastic nature of supply generation and demand levels, and deterministic edge capacities. We let $\mathcal{S}_R \subseteq \mathcal{S}$ be the set of supply node indices having random capacity, and similarly $\mathcal{D}_R \subseteq \mathcal{D}$ be the set of demand node indices having random demand level. Stochastic supply generation and demand levels are introduced to mimic real-life environments better, and randomness in supply and demand is prominent in the existing literature. The stochastic nature of supply is analyzed in different settings such as supply chain networks (Santoso et al., 2005; Govindan et al., 2017) and power networks with renewable energy resources (Poudel et al., 2019; Biswas et al., 2019). Moreover, networks with random demand is studied in the existing literature (Babayan et al., 2005; Hinojosa et al., 2014; Qiu & Wang, 2016).

The objective of the flow-network optimization model is to minimize the total cost with the following components: (i) total cost of flow on edges, (ii) total supply cost, (iii) total cost of unsatisfied demand, (iv) total cost of overload, where each of them are related to the corresponding decisions.

Indices, parameters and decision variables used in the model are given below:

Indices

i : Edge index $\forall i \in \mathcal{E}$

j : Node index $\forall j \in \mathcal{V}$

Parameters

L_j: Demand level of node $j \in \mathcal{D}$

$\bar{G}_j$: Capacity of supply generation at node $j \in \mathcal{S}$

$\bar{P}_i$: Capacity of edge before investment $i \in \mathcal{E}$

Y_j : Unit cost of supply at node $j \in \mathcal{S}$

θ_j: Unit cost of unsatisfied demand at node $j \in \mathcal{D}$

β_i : Unit cost of flow on edge $i \in \mathcal{E}$

ρ_i: Unit cost of overload on edge $i \in \mathcal{E}$

c_i: Additional edge capacity (investment) for edge $i \in \mathcal{E}$

$v_{ij}: \begin{cases} 1, & \text{if edge } i \text{ is outgoing from node } j \\ -1, & \text{otherwise} \end{cases}$

Decision Variables:

g_j: Supply at node $j \in \mathcal{S}$

y_j: Fraction of satisfied demand at node $j \in \mathcal{D}$

p_i : Flow on edge $i \in \mathcal{E}$

s_i: Overload on edge $i \in \mathcal{E}$

The flow-network optimization model below, takes as an input graph $\mathcal{G}$, an instance of $\mathcal{X} = \left(L_j, \bar{G}_j, \bar{P}_i\right)$, $\forall j \in \mathcal{V}$ and $\forall i \in \mathcal{E}$, and additional edge capacity c_i for edge i, and computes the flow in the network as follows:

(FP)

$$\text{Minimize} \quad \sum_{\forall i \,\in\, \mathcal{E}} \beta_i |p_i| + \sum_{\forall j \,\in\, \mathcal{S}} \Upsilon_j g_j + \sum_{\forall j \in \mathcal{D}} \theta_j (1 - y_j) L_j$$

$$+ \sum_{\forall i \,\in\, \mathcal{E}} \rho_i s_i \tag{3}$$

subject to

Flow balance eqn.

$$p_i = g_j \qquad\qquad \forall j \in \mathcal{S}, \forall i \in \mathcal{E}_j \tag{4}$$

$$p_i = y_j L_j \qquad\qquad \forall j \in \mathcal{D}, \forall i \in \mathcal{E}_j \tag{5}$$

$$\sum_{i \in \mathcal{E}} v_{ij}\, p_i = 0 \qquad\qquad \forall j \in \mathcal{I} \tag{6}$$

Capacity const.

$$-(\bar{P}_i + c_i + s_i) \le p_i \le (\bar{P}_i + c_i + s_i) \qquad \forall i \in \mathcal{E} \tag{7}$$

$$0 \le g_j \le \bar{G}_j \qquad\qquad \forall j \in \mathcal{S} \tag{8}$$

Boundary const.

$$0 \le y_j \le 1 \qquad\qquad \forall j \in \mathcal{D} \tag{9}$$

$$0 \le s_i \qquad\qquad \forall i \in \mathcal{E}. \tag{10}$$

We define $\mathcal{E}_j$ is the set of edges that connected to node $j \in \mathcal{V}$ such that $\mathcal{E} = \cup_j \mathcal{E}_j$. The bidirectional edges between intermediate nodes are assigned with arbitrary reference directions for modeling purposes. Hence, flow on these edges are allowed to take both negative and positive values, bounded by the edge capacity $\bar{P}_i$. For a well-defined flow problem, we assume total supply generation capacity is greater than or equal total demand, i.e., $\sum_{j \in \mathcal{S}} \bar{G}_j \ge \sum_{j \in \mathcal{D}} L_j$.

Constraints (4) and (5) determine supply generation at node $\forall j \in \mathcal{S}$ and satisfied demand level at node $j \in \mathcal{D}$, respectively. The flow balance on intermediate nodes are satisfied by constraint (6). Constraints (7) and (8) are capacity constraints for flow on edge $i \in \mathcal{E}$ and supply generation at node $j \in \mathcal{S}$. Finally, constraints (9) and (10) set boundaries for fraction satisfied demand and overload (slack variable).

The objective function (5) of the flow-network model *(FP)* provides a flexible structure that can be adapted to different real-life applications by tuning the unit cost

22

parameters. For example, for the cases where all demand should be satisfied and shortages are not allowed, setting θ_j very large would yield solutions with $y_j = 1$. On the other hand, for cases where overloading the edges is not possible, one should set ρ_i to a very large value.

Thus far, we have modeled an instance of the flow-network defined by $\mathcal{G}$ and the flow optimization model written for a certain realization of random supply and demand. When the system is working under nominal conditions, there is neither over capacity requirement nor unsatisfied demand, i.e., the designed network is capable to run the system satisfactorily. We now consider that the network is inherently prone to cascaded failures triggered by shocks (initial edge failures). We model the initial edge failures by 0-1 Bernoulli random variable, $\kappa = \{\kappa_i\}$ for $\forall i \in \mathcal{E}_I$ where $\mathrm{P}\,(\kappa_i = 1)$ is the probability that an intermediate edge experiences an initial shock. Edge that experienced shock is removed from $\mathcal{G}$ and will not recover until the system reaches equilibrium. In case of an edge failure, the propagation mechanism proceeds as follows. After an initial failure, the flow problem *(FP)* is solved and overloaded edges $\{s_i > 0)$ are failed and, hence, these edges are removed from the graph. This continues until the system reaches an equilibrium when there is no new edge failure. At the end of these iterations, DNS is calculated as the main output for the systemic risk measure.

We let Ω be the finite set of scenarios defined by an instance $\mathcal{X}$ and κ which corresponds to random supply and demand, and initial failures, respectively. For each scenario $\omega \in \Omega$, we let $q(\omega)$ denote the probability of the particular scenario ω. We illustrate the simulation process of the initial edge failures with the flowchart in Figure 4.2., and DNS under scenario ω is calculated using equation,

$$\sum_{\forall j \in \mathcal{D}} \left(1 - y_j^*(\omega, c)\right) L_j(\omega) \qquad (11)$$

where $y_j^*(\omega, c)$ is the optimal fraction of satisfied demand at demand node j, obtained from the solution of *(FP)* given the additional edge capacity vector $c = \{c_i\}$ for $i \in \mathcal{E}$.
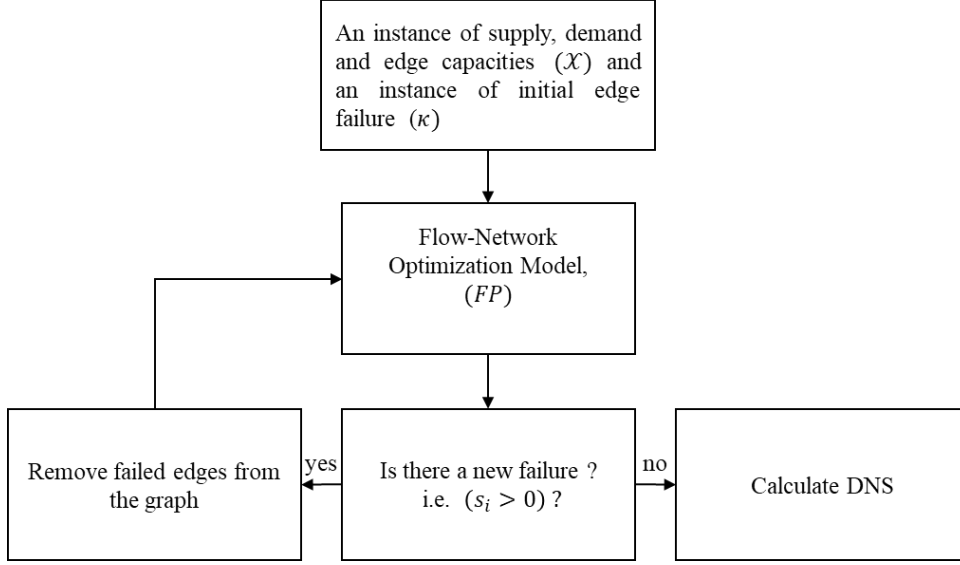
Figure 4.2. Flowchart of the Failure Propagation Simulation

Next, we construct a systemic risk measure that finds the edge capacities satisfying a certain service level.

4.2. Systemic Risk Measure

In the study of Feinstein et al. (2017) systemic risk measure is defined with a random variable called as *aggregation function* Λ that describes a system-wide performance metric such as service level, resilience, profit, cost etc., and an *acceptability criterion* $\mathcal{A}$ that defines the subset of the random variables that are acceptable to the regulator of the system according to a certain criterion. In this thesis, we select Λ defined using DNS that depends on network topology $\mathcal{G}$, an instance of random supply, demand and deterministic edge capacities $\mathcal{X}$, random initial failure κ and the additional edge capacity vector c, *i.e.,* $\Lambda(\mathcal{G}, \mathcal{X}, \kappa, c)$. We consider ξ as the DNS risk level and α as the corresponding probability risk level, and we define acceptability as the probability that DNS is above a certain threshold ξ is within the tolerable limit α.

The systemic risk measure is constructed from *aggregation function* and the notion of *acceptability* as follows,

$$R(\mathcal{G}, \mathcal{X}, \kappa) = \{c \in \mathbb{R}^n_{\geq o} \mid \Lambda(\mathcal{G}, \mathcal{X}, \kappa, c) \in \mathcal{A}\} \qquad (12)$$

$$= \{c \in \mathbb{R}^n_{\geq o} \mid P(\Lambda(\mathcal{G}, \mathcal{X}, \kappa, c) \geq \xi) \leq \alpha\} \quad (13)$$

We let Ω_r be the set of scenarios under which resulting DNS is more than predetermined threshold level as follows:

24

$$\Omega_r(c) = \{\omega \in \Omega \mid \sum\nolimits_{\forall j \in \mathcal{D}} \left(1 - y_j^*(\omega, c)\right) L_j(\omega) \geq \xi\}. \quad (14)$$

Embedding (12) into equation (11) yields the following equation,

$$R(\mathcal{G}, \mathcal{X}, \kappa) = \{c \in \mathbb{R}_{\geq o}^n \mid \sum_{\omega \in \Omega_r(c)} q(\omega) \leq \alpha\}. \quad (15)$$

Systemic risk measure $R(\mathcal{G}, \mathcal{X}, \kappa)$ corresponds to the feasible region of our capacity expansion optimization model. If, for a particular c, none of the scenarios result in a DNS that is above the threshold, then the set $\Omega_r(c)$ would be the empty set, and c would be included in $R(\mathcal{G}, \mathcal{X}, \kappa)$ directly from (15). There is a monotone relationship between DNS and additional edge capacity c such that DNS is non-increasing in c. We employ a grid search algorithm (GSA) that is designed exploit such monotonicity property to compute systemic risk measure $R(\mathcal{G}, \mathcal{X}, \kappa)$ in (15) as detailed in Chapter 5.1. In the next chapter, we build the capacity expansion optimization model considering the risk measure presented in this chapter as the constraints of the model.

4.3. Capacity Expansion Optimization Model

We pose the problem of finding cost-optimal edge capacity expansion plan over $\mathcal{G}$ as a stochastic optimization model:

$(P4.1)$

$$\begin{aligned}
&minimize && \eta(c) && (16)\\
&subject\ to && P(\Lambda(\mathcal{G}, \mathcal{X}, \kappa, c) \geq \xi) \leq \alpha && (17)\\
&&& c \in \mathbb{R}_{\geq o}^n, && (18)
\end{aligned}$$

where the non-negative decision vector $c = [c_1, c_2, \dots, c_n] \in \mathbb{R}_{\geq o}^n$ is the additional edge capacity. The objective function $\eta(c) \in \mathbb{R}$ represents the monetary value of the decision c. Note here that, since we divide edges into two groups, $n = 2$. The systemic risk measure (13) is embedded into $(P4.1)$ such that it defines a feasibility condition that guarantees the probability of DNS is above a certain threshold (ξ) is within the tolerable limit α, for a nonnegative solution. Hence, the choice of ξ and α is critical since they determine the feasible region for c, and, consequently, the optimal cost.

Optimization problem $(P4.2)$ can equivalently be stated using (15) as follows:

$(P4.2)$

$$minimize \quad \eta(c) \tag{19}$$

$$subject\ to \quad \sum_{\omega \in \Omega_r(c)} q(\omega) \leq \alpha \quad (20) \rbrace\ \text{probabilistic const.}$$

$$c \in \mathbb{R}^n_{\geq o}. \quad (21) \rbrace\ \text{boundary const.}$$

The structure of the model $(P4.2)$ is suitable to test several cost functions that can be either linear or nonlinear. Although use of linear cost functions are prominent in the literature (Fang et al., 2014; Cassidy et al., 2016), the strength of our approach is the capability to handle general nonlinear cost structures. If we would consider a monotone increasing cost function than apparently cost-optimal solution will be at the boundary of the feasible region, since increasing c_1 and/or c_2 corresponds to increasing $\eta(c)$.

Note that, use of the systemic risk measure with a tractable computation procedure decreases our search space from $\mathbb{R}^n$ to the feasible region which decreases our computation time as well. From the optimization perspective, since constraint handling are done prior to the objective function calculation, the problem complexity is reduced significantly.

In the next chapter, we provide the details of our solution approach for $(P4.2)$. We use a grid search algorithm to find an approximation for the feasible region of the optimization problem $(P4.2)$ (Chapter 5.1). Then, cost-optimal capacity expansion is found using DE (Chapter 5.2).

,

CHAPTER 5
SOLUTION APPROACH

In this study, our solution approach is based on an iterative methodology which first identifies the feasible region dictated by the model constraints $(20 - 21)$, and then, finds the optimal solution of the minimization capacity expansion optimization problem $(P4.2)$. The flowchart of the solution approach is represented in Figure 5.1. Given an initial flow-network, we first group edges as detailed in Chapter 3.3. Next, a grid search algorithm is run to identify the feasible set of the $(P4.2)$. We address the stochastic nature of supply and demand $\mathcal{X}$ (Chapter 3.1) and initial edge failures κ (Chapter 3.2) by employing Monte-Carlo simulations within a grid search algorithm. Given a nonnegative additional edge capacity c, the model is solved for every scenario ω, and empirical distribution of DNS is obtained. After that, probabilistic constraint is checked. The iteration starting with candidate c repeats until feasible region is determined (Chapter 5.2). Then, this feasible region is used to create initial population of the population-based heuristic algorithm DE, as explained in Section 5.3. The cost-optimal capacity expansion and corresponding cost are calculated at the final step.
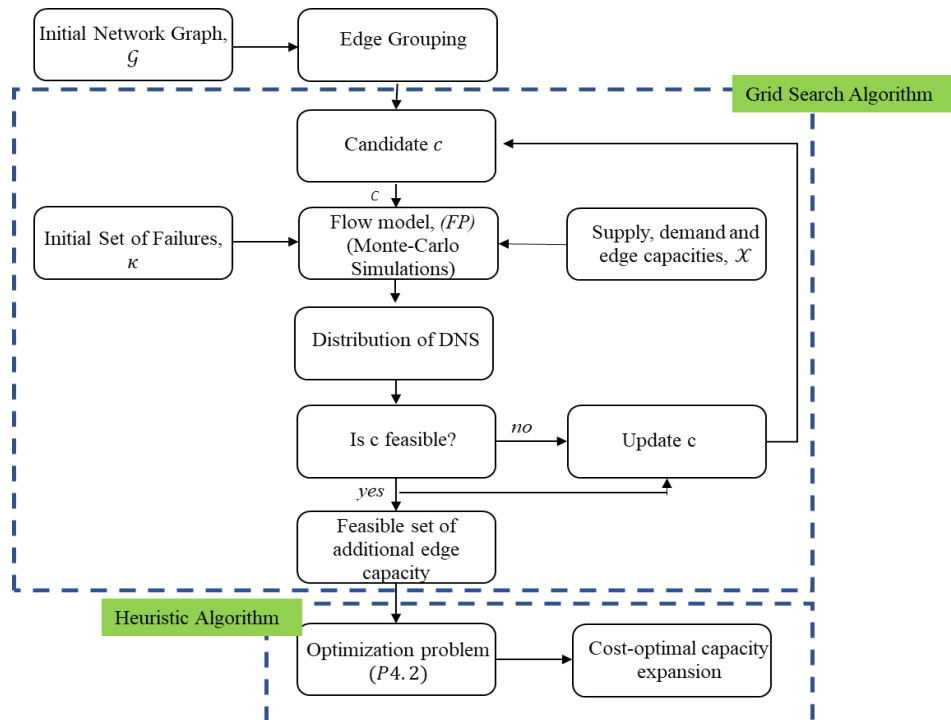

Figure 5.1. Flowchart of the Solution Methodology: The Steps to Find Cost-Optimal Additional Edge Capacities.

5.1. Grid Search Algorithm

In our study, feasible region, which are the additional edge capacities that satisfy the probabilistic constraint (20) and boundary constraint (21), is determined using the distribution of DNS given a candidate c. Furthermore, there is a monotone relationship between DNS and additional edge capacity c (DNS is non-increasing in c). Thanks to this monotonicity property, finding the feasible region is reduced down to determining the boundary of this region. We employ a grid search algorithm (GSA) (Feinstein et al., 2017) that is designed exploit such monotonicity property, and to find the boundary of the feasible region efficiently. In order to find c values satisfying probabilistic constraint, at every iteration of GSA, flow model (FP) coupled with Monte-Carlo simulations is run.

The main steps of GSA are illustrated in Figure 5.2. Since edges are divided into 2 groups as detailed in Chapter 3.3, in GSA, the region of additional edge capacities is approximated by a 2-dimensional grid bounded by minimum and maximum allowable additional edge capacities. The accuracy for approximation of the feasible set and run-time of the algorithm are directly affected by the grid size selection.

Given a grid and an unknown feasible region boundary, GSA starts by moving along the diagonal in direction $[1\ 1]^{\mathrm{T}}$ until it finds the first feasible grid point c_{int} in this direction (Figure 5.2.a.). Then, the grid is divided into 4 quadrants centered at c_{int}. Due to monotonicity, all the grid points in Quadrant-I are feasible, whereas all the grid points in Quadrant-III except from the boundary of the same quadrant are infeasible (Figure 5.2.b.). Feasible grid points in Quadrant-II are determined as follows: Starting with c_{int}, if the current grid point is feasible, GSA moves horizontally to the immediate neighbor on the left. Otherwise, if infeasible, GSA moves vertically to the immediate neighbor on the top. In a similar fashion as seen in Figure 5.2.c., in Quadrant-IV, if the current point is feasible, GSA moves vertically to the immediate neighbor on the bottom. Otherwise, if infeasible, GSA moves horizontally to the immediate neighbor on the right. The algorithm stops when it hits the grid boundaries on Quadrant-II and IV. Finally, the feasible points visited by GSA and the other feasible points identified by monotonicity property constitute the approximation of the feasible region as given in Figure 5.2.d.

a. Diagonal Search

b. Quadrant Division

c. Move in Quadrant-II and IV

d. The Final Grid
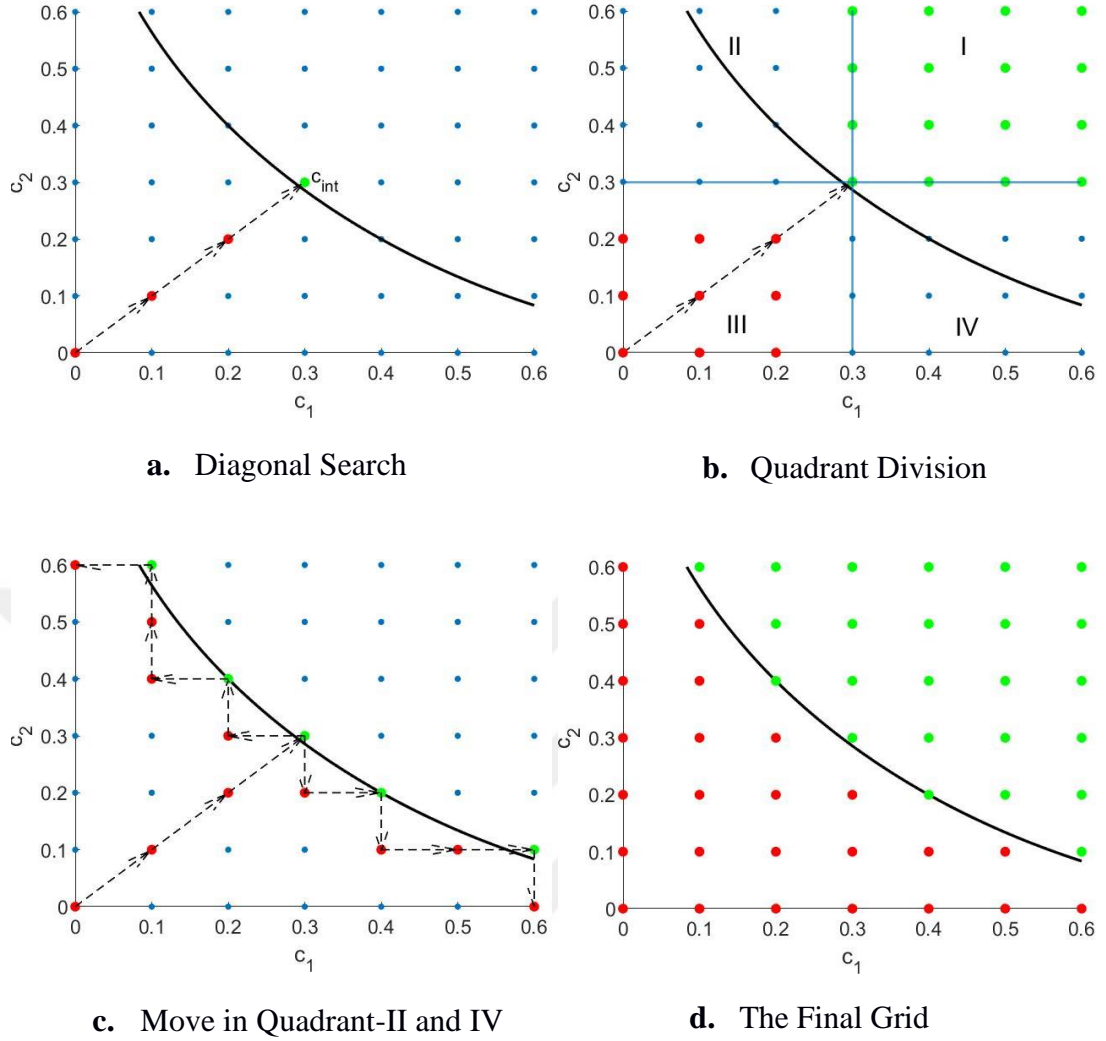
Figure 5.2. Demonstration of the GSA Steps

5.2. Heuristic Algorithm

After determination of the feasible region, cost-optimal capacity expansion is found using a heuristic algorithm, namely DE. Cost of capacity expansion can be modeled in various ways depending on the specific application. In this thesis, we consider the cost function given in (22) that captures immediate cost of investment and the cost of future risk. This is an exemplary cost function that is inline with our problem environment, other cost structures can also be employed in our problem.

$$\eta(c) = (k_1 c_1 + k_2 c_2 + Q_1 \phi_1 + Q_2 \phi_2) + k_3 \left(1 - e^{-\lambda(c_1, c_2)\Theta}\right) \quad (22)$$

In (22), the first component given in parentheses is the immediate cost. The first two cost factors k_1 and k_2 represent per unit cost of additional capacity, while Q_1 and Q_2 are fixed costs that are incurred when $c_i > 0$, that is, for $i = 1,2$:

$$\phi_i = \begin{cases} 1, & c_i > 0 \\ 0, & c_i = 0. \end{cases}$$

The second component is to account for the future cost of the decision. We penalize the probability that the new system with the expanded capacity fails to achieve probabilistic constraint due to system evolution such as, changes in the supply and demand characteristics, degradation in edge quality/capacity, etc., before the next planned capacity expansion investment in the future. To formulate this, let T denote the time until the probabilistic constraint is not satisfied in the future for selected $[c_1 \ c_2]$ such that,

$$E[\text{T}] = \frac{1}{\lambda(c_1, c_2)}, \qquad (23)$$

and Θ be the time until the next capacity expansion study (known *a priori*). In our study, we assume that T is exponentially distributed with rate

$$\lambda(c_1, c_2) = \frac{1}{c_1} + \frac{1}{c_2} \qquad (24)$$

which is decreasing in c_1 and c_2. Under these definitions, the probability of the future risk can be calculated as,

$$P(\text{T} < \Theta) = 1 - e^{-\left(\frac{1}{c_1} + \frac{1}{c_2}\right)\Theta}, \quad (25)$$

and then, the monetary value of the calculated risk is

$$k_3 \left(1 - e^{-\left(\frac{1}{c_1} + \frac{1}{c_2}\right)\Theta}\right). \qquad (26)$$

One of the main contributions of our study is the flexibility to handle general edge capacity expansion cost structures such as the one given above. To the best of our knowledge, the majority of the related literature assumes simpler cost structures (Fang et al., 2014; Cassidy et al., 2016; Salomon et al., 2020).

In order to solve capacity expansion problem $(P4.2)$ with general cost structures, in this study, we employ a well-known population-based heuristic algorithm, differential evolution (DE). DE has good convergence properties (Storn & Price, 1997), and can handle both discrete and continuous decision variables efficiently. The algorithm starts with an initial population of size N (with each member being n dimensional), and

continues with mutation, cross-over and selection operations at each generation $g = 1,2,\ldots,g_{max}$ until a stopping criterion is met.

Mutation

In the mutation phase, for each individual x_g^j of the current population (called as target vector), a mutant vector v_g^j is generated for $j = 1,2,\ldots,N$. There are various mutation strategies used in the literature (Mallipeddi et al., 2011).

In this study, for each target vector, three individuals $x_g^{j_a}$, $x_g^{j_b}$ and $x_g^{j_c}$ from the population are randomly selected, and the mutant vector is calculated as follows:

$$v_g^j = x_g^{j_a} + F\left(x_g^{j_b} - x_g^{j_c}\right), \quad (27)$$

where F is a scaling factor, and usually chosen within the range [0.5,1] (Storn, 1996).

Cross-over

Cross-over operation increases the diversity of the population. At this step, the trial vector $u_g^j = \{u_{ig}^j\}$ for $i = 1,2,\ldots,n$ is generated by applying a uniform cross-over to $x_g^j = \{x_{ig}^j\}$ and $v_g^j = \{v_{ig}^j\}$ as follows:

$$u_{ig}^j = \begin{cases} v_{ig}^j & \text{if } r_{ig}^j \leq CR \\ x_{ig}^j, & \text{otherwise} \end{cases} \quad (28)$$

where $r_{ig}^j \sim U(0,1)$ and CR is the user specified cross-over rate in [0 1].

Selection

At this step, target and trial vectors are compared with regard to a fitness function $f(\cdot)$, and *elitist* selection is applied to select a new individual for the next generation as follows:

$$x_{g+1}^j = \begin{cases} x_g^j, & \text{if } f(u_g^j) \leq f(x_g^j) \\ u_g^j, & \text{otherwise.} \end{cases} \quad (29)$$

These three consecutive steps are repeated for each individual in the current population, and the next generation is populated until a stopping criterion is reached. The optimal solution of the problem is then the individual of the last generation which has the lowest fitness value. In this study, we use the following DE parameters: $N = 100$, $g_{max} = 250$, $F \sim U(0.2, 0.8)$, $CR = 0.6$.

In the next chapter, we introduce the values of the system parameters and test instances for numerical study, and report our findings on the effects of system parameters on the feasible region and cost.

CHAPTER 6
COMPUTATIONAL STUDY

To test our solution approach, we apply proposed framework to a medium-size network. In this section, we report the results of our numerical study that we perform using MATLAB (R2016b). Required computational time for the solution of flow-network optimization problem (FP) is less than 1 sec, and we require 30-45 min. for the check of probabilistic constraint of each grid point. Since computation of the feasible region depends on both the required time for probabilistic constraint check of each grid point and the number of points checked, there is not any exact computation time to identify feasible region. Finally, differential evolution (DE) requires approximately 5 sec. to find the solution if the maximum number of generations g_{max} is selected as 250.

In particular, we perform an extensive numerical study which aims to show the applicability of our framework to a general flow-network, and investigate the followings.

i. The objective function of the flow-network model (FP) provides a flexible structure that can be adapted to different real-life applications by tuning the unit cost parameters where these parameters might affect the feasible region.

ii. Eigenvector centrality and utilization-based edge grouping result to different edge group assignments. We claim that as eigenvector centrality depends solely on the network topology where the more centralized edges (according to eigenvector centrality) tend to be in close proximity, the resulting feasible region highly depends on the group assignments of initially failed edges. The utilization-based group assignment depends on the network topology, supply and demand characteristics, edge capacities and flow-network optimization model. Consequently, when we employ utilization-based initially failed edge selection in our numerical experiments, the risk of decreasing c_1 is more than c_2. Hence, more c_2 is required to decrease c_1 compared to required c_1 to decrease c_2.

33

iii. We conjecture that supply and demand characteristics directly affect the feasible region and hence, the optimal solution. Both the location of the random supply and the parameters of the supply generation would affect the set of admissible edge capacities under the same demand distribution and parameters. Demand distribution and parameters determine the sample space (scenarios) and the corresponding probability of the scenarios. We claim that the increase in sample space range or right tail probabilities for random demand nodes under the same sample space leads to shrinkage in the feasible region.

iv. We employ two different selection method for initially failed edges: random and utilization-based. Random failures affect any random edge, whereas in utilization-based method the initially failed edges the most expected failures starting from the highest-load. As a result, we foresee that the resulting feasible region will be larger in random initially failed edge selection.

v. DNS and risk thresholds, ξ and α, respectively, are the parameters of the probabilistic constraint which is used to define the feasibility. As a result, these parameters directly affect the feasible region. We claim if we increase ξ and α, feasible region stays same or enlarges.

In Chapter 6.1., we introduce network topology, network parameters, cost parameters of the flow-network optimization problem (FP) and capacity expansion optimization problem ($P4.2$) and test instances for numerical experiments. Then, we discuss our findings in Chapter 6.2.

6.1. Values of the System Parameters and Test Instances

We conduct our numerical experiments on a representative flow-network illustrated in Figure 6.1.
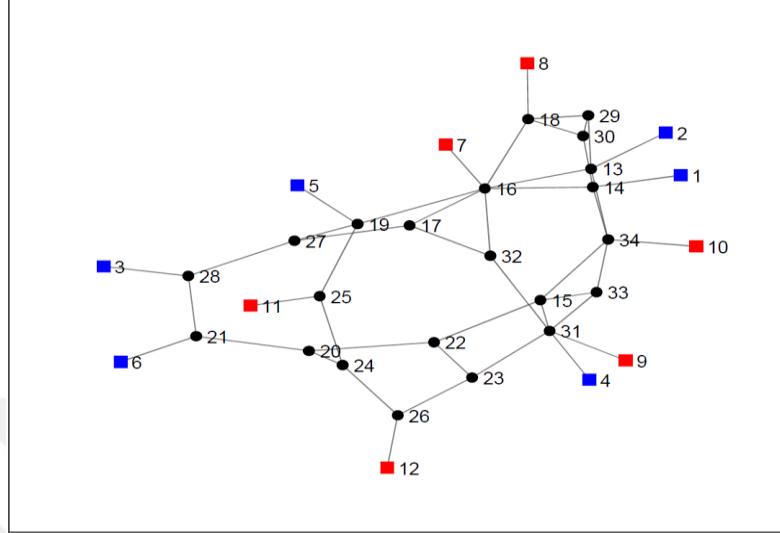
Figure 6.1. Network Graph. Square Blue Nodes Demonstrate Supply Nodes, Square Red Nodes Show Demand Nodes and Circle Black Nodes denote Intermediate Nodes.

In this network, there exist 34 nodes ($|\mathcal{V}| = 34$) and 46 edges ($|\mathcal{E}|=46$). The network has 6 demand nodes ($|\mathcal{D}| = 6$), 6 supply nodes ($|\mathcal{S}| = 6$) and 22 intermediate nodes ($|\mathcal{I}| = 22$). We assume that one of the supply nodes have stochastic capacity, and demand levels of the two demand nodes are random. We assume that random supply node is distributed *d-normal* with parameters (μ_j, σ_j) for random supply node j, for $j \in \mathcal{S}_R$. Whereas, random demand nodes j are distributed either *d-normal* (μ_j, σ_j) or *d-uniform* $[\mu_j - 2\sigma_j, \mu_j + 2\sigma_j]$. The number of equal length intervals for *d-normal* and *d-uniform* distribution is 4, i.e., $n_{int} = 4$. Hence, the number of corresponding boundary points of the bins are 5, and hence, the number of scenarios generated for each random node is 5. This leads to $5^1 = 5$ different supply generation scenarios and $5^2 = 25$ demand level scenarios. The mean and standard deviation of *d-normal* supply generation and demand levels (μ_j, σ_j), and the ranges for *d-uniform* demand levels $[\mu_j + 2\sigma_j, \mu_j - 2\sigma_j]$ are given in columns 2 and 5, respectively in Table 6.1. Note that, the nodes with deterministic supply generation or demand level are represented with 0 standard deviation, i.e., $\sigma_j = 0$. Moreover, unit cost of supply

generation (γ_j) and unsatisfied demand (θ_j) are given columns in 3 and 6, respectively in Table 6.1. The cost of generation for the supply node with stochastic capacity is assumed to be negligible compared to the other supply nodes. One example for such a case would be renewable (wind, PV) generation in power networks.

As we consider a general flow-network, the parameters, and hence the results are unitless in the numerical experiments.

TABLE 6.1. Supply and Demand Parameters

Supply			Demand		
$j \in \mathcal{S}$	(μ_j, σ_j)	γ_j	$j \in \mathcal{D}$	$(\mu_j, \sigma_j) / [\mu_j + 2\sigma_j, \mu_j - 2\sigma_j]^\dagger$	θ_j
1	$(60, 50)$	0	7	$(65, 10) / [45,85]$	$1e+07$
2	$(80, 0)$	50	8	$(65, 10) / [45,85]$	$1e+07$
3	$(85, 0)$	50	9	$(65, 0) / [65,65]$	$1e+07$
4	$(80, 0)$	50	10	$(60, 0) / [60,60]$	$1e+07$
5	$(95, 0)$	50	11	$(50, 0) / [50,50]$	$1e+07$
6	$(70, 0)$	50	12	$(50, 0) / [50,50]$	$1e+07$

† The distribution of the demand level is either *d-normal* with parameters (μ_j, σ_j) or *d-uniform* with parameters $[\mu_j + 2\sigma_j, \mu_j - 2\sigma_j]$.

The capacities ($\bar{P}_i$) of the intermediate edges are randomly assigned to 45, 50 and 55. The supply and demand edges are introduced for modeling purposes, and are given very large capacity ($1e+05$) compared to intermediate edges between. In Appendix I, the capacities that are assigned to each edge is given in detail. In our experiments, only intermediate edges ($i \in \mathcal{E}_I$) are subjected to capacity expansion, and initially failed edges are also selected among these edges (34 edges in total). The two costs associated with the edges in (FP) are same for supply, demand and intermediate edges, and are taken as $\beta_i = 1$ and $\rho_i = 1e+03$, for the unit cost of flow and overload, respectively.

We define the set of initially failed edges under the subset $\mathcal{E}_{IF} \subset \mathcal{E}$. The selection methodology and probability assignment to the initially failed edges are explained in Chapter 3.2. The maximum number of edges that are exposed to initial shocks simultaneously are taken to be 10% of total number of edges that can fail. Therefore, in our network, the number of initially failed edges is less than or equal to 4 depending on the scenarios generated, i.e., $|\mathcal{E}_{IF}| \leq 4$. In total, there are $2^4 = 16$ initial failure scenarios which composed of 1 no initial failure, 4 single line failures, 6 two

simultaneous edge failures, 4 three simultaneous edge failures and 1 four simultaneous edge failure scenarios. Overall, given a nonnegative additional edge capacity $c = [c_1\ c_2]$,i.e., $c_1 \geq 0$ and $c_2 \geq 0$, we run 2000 Monte-Carlo simulations to find the distribution of DNS and check probabilistic constraint as detailed in Table 6.2. below.

TABLE 6.2. Number of Scenarios

Random Supply Amount	Random Demand Level	Initial Edge Failure	Total
5^1	5^2	2^4	2000

The parameters of the objective function of the problem $(P4.2)$ (cost function (22)) are given in Table 6.3. Moreover, in the numerical studies, ξ is selected as 10% of the expected total demand $\sum_{j \in \mathcal{D}} \mu_j$, and α is selected as 0.05. The parameters introduced thus far were at nominal conditions, and are referred to as base case parameters hereafter.

TABLE 6.3. Objective Function $(\eta(c))$ Parameters

| k_1	k_2	k_3	Q_1	Q_2	Θ
150	190	5000	750	1900	1

For the numerical experiments, the test instances (TI) in Table 6.4. are used throughout this chapter. In this table, diamond ($\diamond$) represents base case parameter, whereas star ($\star$) shows a change in the parameter.

<p style="text-align:center;">**TABLE 6.4.** Test Instances (TI)</p>

	Edge Grouping	Initial Failure Probability of Edge i, $i \in \mathcal{E}_{IF}$	Supply Characteristics	Demand Characteristics	ξ	α
$TI1$	eig. centrality	0.1	◇	◇	◇	◇
$TI2$	util. based	0.1	◇	◇	◇	◇
$TI3$	util. based	0.1	◇	★	◇	◇
$TI4$	eig. centrality	$0.1(ur_i/\Sigma ur_j)$	◇	◇	◇	◇
$TI5$	util. based	$0.1(ur_i/\Sigma ur_j)$	◇	◇	◇	◇
$TI6$	eig. centrality	0.1	★	◇	◇	◇
$TI7$	eig. centrality	0.1	◇	★	◇	◇
$TI8$	util. based	$0.1(ur_i/\Sigma ur_j)$	◇	◇	★	◇
$TI9$	util. based	$0.1(ur_i/\Sigma ur_j)$	◇	◇	◇	★

6.2. Results

In this part, we demonstrate the feasible region boundaries resulting from various experiments using test instances in Table 6.4., and we discuss the effect of parameter changes on decision, and hence, cost. The feasible region boundary provide approximation to the feasible set of additional edge capacity c (each c corresponds to a grid point in GSA). For each additional edge capacity vector c, the sum of the probabilities of total demand-not-satisfied (DNS) that are above a certain threshold (ξ) is compared to the risk threshold α. A grid point is said to be feasible is sum of the probabilities of DNS that are above ξ is less than α, and not feasible, otherwise. see Figure 6.2.a. for an illustrative example of DNS distribution for a feasible grid point, and see Figure 6.2.b. for an infeasible example.

a. Feasible c **b.** Infeasible c
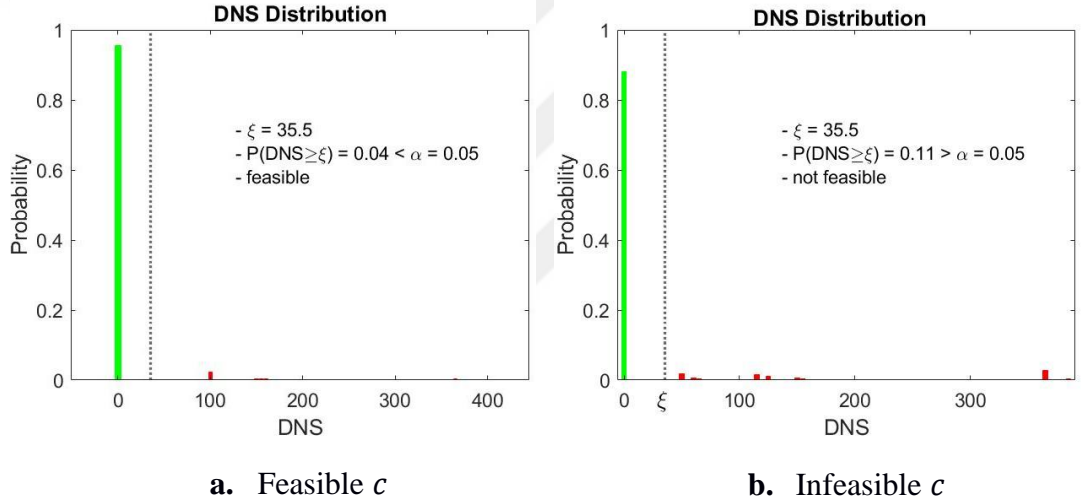
Figure 6.2. Distribution of DNS for a Given Additional Edge Capacity c.

In the following subchapters, we discuss the effect of system parameters on the resulting feasible region and cost of the optimal capacity expansion.

### 6.2.1. Effects of Changes in Flow-Network Model Parameters

The objective function of the flow-network model (FP) given below is composed of total cost of flow on edges ($\sum_{\forall i \in \mathcal{E}} \beta_i |p_i|$) , total supply cost ($\sum_{\forall j \in \mathcal{S}} Y_j g_j$), total cost of unsatisfied demand ($\sum_{\forall j \in \mathcal{D}} \theta_j (1 - y_j) L_j$) and total cost of overload ($\sum_{\forall i \in \mathcal{E}} \rho_i s_i$). For every cost component, there is a decision variable and corresponding cost parameter.

$$\sum_{\forall i \in \mathcal{E}} \beta_i |p_i| + \sum_{\forall j \in \mathcal{S}} Y_j g_j + \sum_{\forall j \in \mathcal{D}} \theta_j (1 - y_j) L_j + \sum_{\forall i \in \mathcal{E}} \rho_i s_i$$

The function given above provides a flexible structure that can be adapted to different real-life applications by tuning the unit cost parameters. For example, for the cases where all the demand should be satisfied and shortages are not allowed, setting the unit cost of unsatisfied demand (θ_j) on edge $j \in \mathcal{D}$ very large would yield solution where the fraction of satisfied demand is equal to 1, i.e., $y_j = 1$. On the other hand, if service level requirement is not very high (unsatisfied demand is allowed), one can set θ_j is relatively small. Moreover, for cases where overloading the edges $(s_i > 0)$ is not possible, one should set the unit cost of overload ρ_i to a very large value.

Figure 6.3 below shows the resulting feasible region boundaries for different θ_j and ρ_i, in $TI1$. As given in Figure 6.3.a., we first run GSA for three different θ_j under the same ρ_i, where $\theta_j = 1e + 07$ in the base case, and we test $\theta_j = 1e + 02$ and $\theta_j = 1e + 12$. Figure 6.3.a. shows that the current system is capable enough to satisfy probabilistic constraint (20), which is $(\sum_{\omega \in \Omega_r(c)} q(\omega) \leq \alpha)$, when the penalty for shortages are low, i.e., $\theta_j = 1e + 02$. Intuitively, in this case, failure cascades can be stopped at earlier stages by allowing some unsatisfied demand, and hence, failure is not propagated through the entire system. Next, we test the base case where $\theta_j = 1e + 07$. We observe that feasible region shrinks with the increase in θ_j. Finally, we set θ_j to a very large number, i.e., $\theta_j = 1e + 12$, to demonstrate the problem environments where demand shortages are not allowed. We observe that, this case yields no feasible solution on the grid as given in Figure 6.3.a. This implies that if we do not allow shortages at earlier stages, cascading failures might not be stopped until a complete failure if edge capacities are not very high. In real-life there can be very high service level requirements (the cost of unsatisfied demand very high), for such cases, it is recommended to increase edge capacities to mitigate the risk of complete failure.

Figure 6.3.b. shows the resulting feasible region of the experiments where we test the effect of change the ρ_i under the same θ_j. We set ρ_i as $0.5e + 03$, $1e + 03$, and $1e + 07$, where $\rho_i = 1e + 03$ is the base case parameter. Figure 6.3.b. reveals that feasible shrinks as we decrease the unit cost of overload ρ_i. We claim that when ρ_i decreases under the same θ_j, system allows more overloads, and hence, failure propagation tend to move further. Hence, the failure propagation might not stop at early stages and result in a larger DNS with smaller ρ_i, compared to larger choice of ρ_i. As a result, risk increases and feasible region shrinks with the decrease in ρ_i.

| **a.** Changes in cost of unsatisfied demand | **b.** Changes in cost of overload |
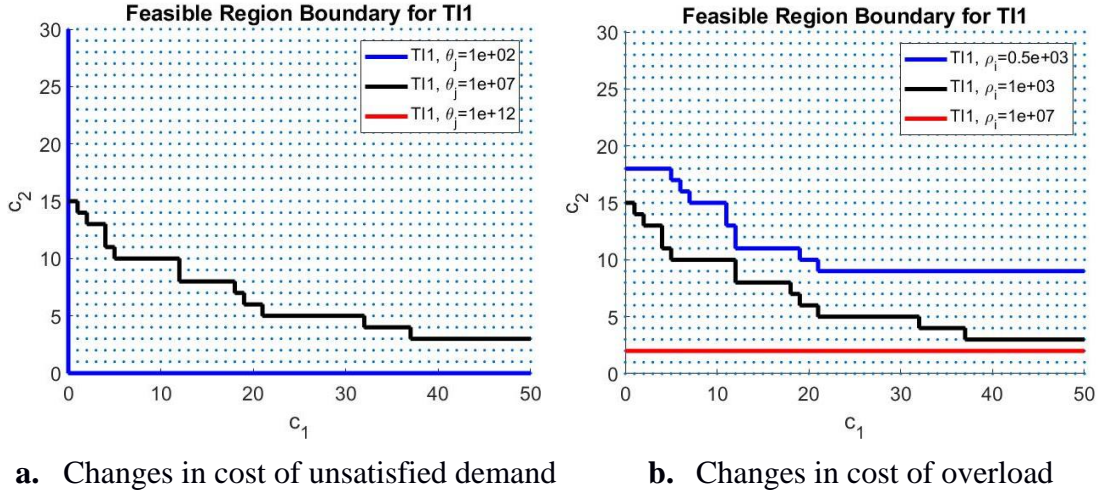
Figure 6.3. Feasible Region Boundaries for Different θ_j and ρ_i.

Table 6.5. shows the optimal capacity expansion and cost for the cases above. Even though the current system is capable enough to satisfy probabilistic constraint (20), it has a risk of not satisfying (20) in the future. Therefore, there exist a cost for future risks as given in the first row of the Table 6.5. We also show that, since feasible region shrinks with the decrease in ρ_i, $\eta(c_{TI1}^*)$ decreases as given in the below table.

TABLE 6.5. Optimal Capacity Expansion and Cost for $TI1$ under different θ_j and ρ_i

θ_j	ρ_i	c_{TI1}^*	$\eta(c_{TI1}^*)$
$1e+02$	$1e+03$	[0.0 0.0]	5000.0
$1e+07$	$1e+03$	[5.0 10.0]	6595.9
	$0.5e+03$	[12.0 11.0]	7339.5
$1e+07$	$1e+03$	[5.0 10.0]	6595.9
	$1e+07$	[4.6 4.1]	5966.6

6.2.2. Effects of Changes in Edge Grouping Method

In this study, we employ two different edge grouping methods as detailed in Chapter 3.3. Figure 6.4. shows group assignments of the edges resulting from eigenvector centrality methods and utilization-based methods, and Table A.2.1. in Appendix II provide more details regarding to edge indices and corresponding groups. For TI1, TI2 and TI3 in Figure 6.4., we illustrate Group-1 edges in green and Group-2 edges in magenta. Group-1 and Group-2 edges in eigenvector centrality are concentrated in

separate regions of the graph. This is expected, since, in eigenvector centrality method, edges with high "importance" tend to be together as a single connected sub-graph. On the other hand, in utilization-based grouping, edges in a certain group are more dispersed throughout the network. The topology of the sub-graphs corresponding to each group is dependent on edge capacities, supply and demand characteristics. For example, compared to Figure 6.4.b., in Figure 6.4.c., mean demand at nodes 7 and 8 are decreased by 10, while mean demand at nodes 9 and 10 are increased by the same amount. The resulting grouping shows that the edges between nodes 31-32, 18-29 and 18-30 switch groups. Eigenvector centrality is, however, dependent only on the network topology, and is invariant to changes in network parameters.
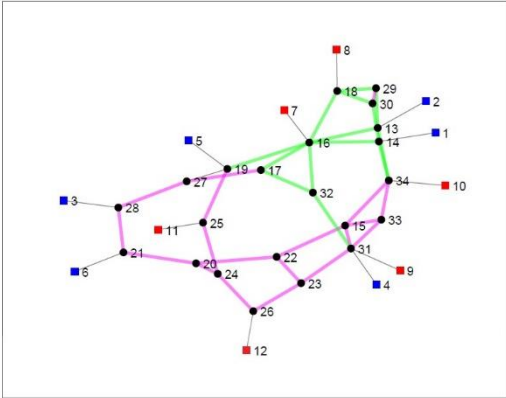
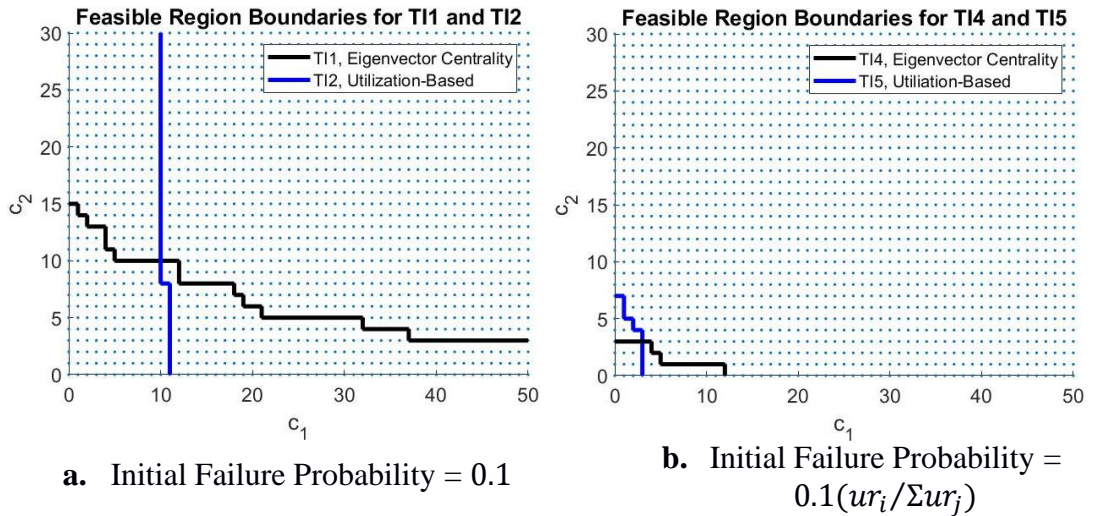**b.** *TI*1, Eigenvector Centrality   **b.** *TI*2, Utilization-Based
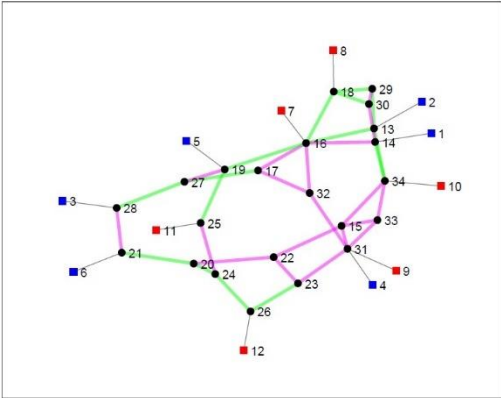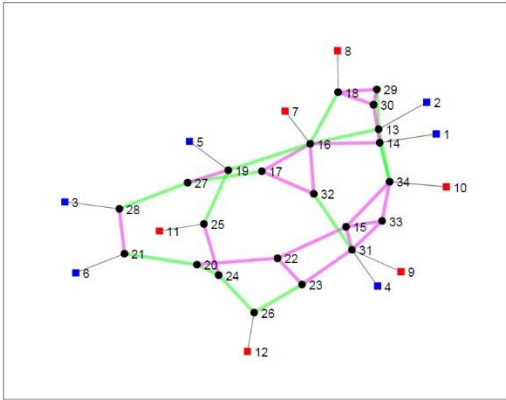
c. *TI*3, Utilization-Based

Figure 6.4. Demonstration of the Edge Group Assignments on the Network Graph. Green Colored Edges are Group-1, whereas Magenta Colored Edges are Group-2.

In order to investigate the effect of edge grouping method on the feasible region, the boundaries of the regions generated by eigenvector centrality and utilization-based methods are compared using $TI1 - TI2$, and $TI4 - TI5$. Different groupings of the two methods result in different feasible region boundaries for $TI1 - TI2$ as given in Figure 6.5.a. Since the eigenvector centrality results in two connected sub-graphs (groups), edges in these sub-graphs are critical for proper functioning of the entire flow network. If any of these groups are subjected to initial shocks, some of the demand nodes may not be adequately served. Since we employ same method to select initially failed edges in all of the test instances used in this experiment ($TI1, TI2$, $TI4,$ and $TI5$), edges between nodes $19 - 25$, $20 - 21$, $16 - 19$ and $17 - 27$ are initially failed. However, these edges fall in different groups in different grouping methods: in $TI1$ and $TI4$ (eigenvector centrality), there is only 1 initially failed edge in Group-1 and 3 edges in Group-2; in $TI2$ and $TI5$ (utilization-based), all of the initially failed edges are in Group-1. Consequently, for $TI1$ there is a trade-off between c_1 and c_2, but c_1 is allowed to be 0, since there is only 1 initially failed edge in Group-1. On the other hand, for $TI2$, c_1 must be above a certain level, to compensate the capacity loss experienced due to initially failed Group-1 edges as shown in Figure 6.5.a.

As given in Figure 6.5.b., a similar trade-off is observed in $TI4$, but unlike $TI1$, both c_1 and c_2 are allowed to be 0. If we consider the points where boundary hits to 0 on both axes, it can be said that c_2 requires more guarantee than c_1, to be 0 (see Figure 6.5.b). On the other hand, we observe the opposite tendency for $TI5$.

a. Initial Failure Probability $= 0.1$

b. Initial Failure Probability $= 0.1(ur_i/\Sigma ur_j)$

Figure 6.5. Feasible Region Boundaries for Eigenvector Centrality and Utilization-Based Edge Grouping.

After finding the feasible regions for $TI1 - TI2$, and $TI4 - TI5$, we solve the capacity expansion optimization problem $(P4.2)$ using DE. In the following table the cost-optimal edge capacity expansions c^* and corresponding costs $\eta(c^*)$ is given.

TABLE 6.6. Optimal Capacity Expansion and Cost for $TI1, TI2, TI4$ and $TI5$

	c^*	$\eta(c^*)$
$TI1$	[5.0 10.0]	6595.9
$TI2$	[11.0 4.4]	6498.6
$TI4$	[4.6 4.1]	5966.6
$TI5$	[4.6 4.1]	5966.6

As given in Table 6.6., c^*_{TI4} and c^*_{TI5} are the same, and hence, $\eta(c^*_{TI4})$ and $\eta(c^*_{TI5})$. On the other hand, c^*_{TI1} and c^*_{TI2} are not even in the feasible region of $TI2$ and $TI1$, respectively. This implies that optimal solution highly depends on the edge grouping method. Therefore, the selection of a proper edge grouping method considering the nature of the specific real-life application is critical.

6.2.3. Effects of Changes in Supply and Demand Characteristics

In this chapter, we investigate the impact of changes in supply characteristics in TI6. We first start with the base case where the random supply is located at node 1, i.e., $S_R = \{1\}$ with capacity distribution *d-normal* $(60,5)$. Keeping the random supply at node 1, we first test another case with a reduced mean of 50, *d-normal* $(50,5)$. As shown in Figure 6.6.a., reduction in random supply mean (while keeping the demand constant) resulted in a narrower feasible region for $S_R = \{1\}$. We conjecture that this behavior is observed, because, when the random supply generation (cost-less, $\gamma_1 = 0$, in flow network (FP)) is reduced, the other (deterministic) supply nodes have to take up the slack, and may cause "congestion" in other parts of the network, which in turn increases the cascading failure risk.

We further conjecture that this phenomenon is also dependent on the location of the random supply node. To test this, we move the location of random supply to the other nodes in separate tests, and recompute the corresponding feasible regions. Nodes $1, 2$ and 4 are at the right section of the graph, especially, nodes 1 and 2 are in close proximity to each other at the upper right section. On the other hand, nodes 3, 5 and 6 are at the left section of the graph and distant from the nodes $1, 2$ and 4. When the

random supply node is located at node 2 (see Figure 6.6.b.) and 4 (see Figure 6.6.d.), the feasible region boundaries for *d-normal* (50,5) and (60,5) are qualitatively similar to Figure 6.6.a. Whereas, we observe no differences in feasible region boundaries for *d-normal* (50,5) and (60,5) at nodes 3 and 5, as given in Figure 6.6.c. and Figure 6.6.e., respectively. In Figure 6.6.f., where the random supply is located at node 6, the relative positions of the feasible region boundaries for *d-normal* (50,5) and (60,5) is opposite of the node 1, 2 and 4. At this case, feasible region shrinks slightly as with the increase in supply mean.

In addition, as random supply is moved between nodes under a certain fixed mean (either 50 or 60), the feasible region boundary also moves. All these observations support our conjecture that the location of the random supply, which is costless, is an important factor for the boundaries of the feasible region. From the perspective of practitioners, for example in power grids, proper selection of the location of renewable sources are critical achieve the global cost-optimal solution for the entire network.
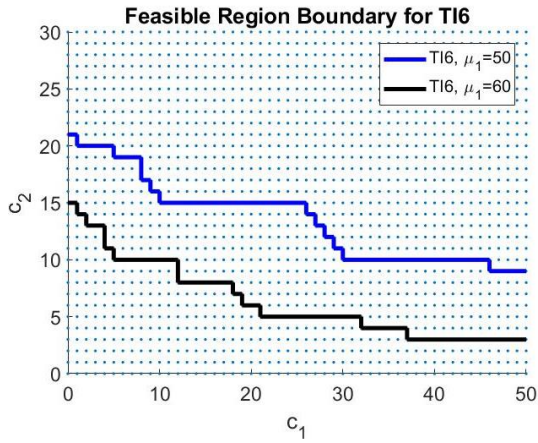
a. Random supply is at node 1
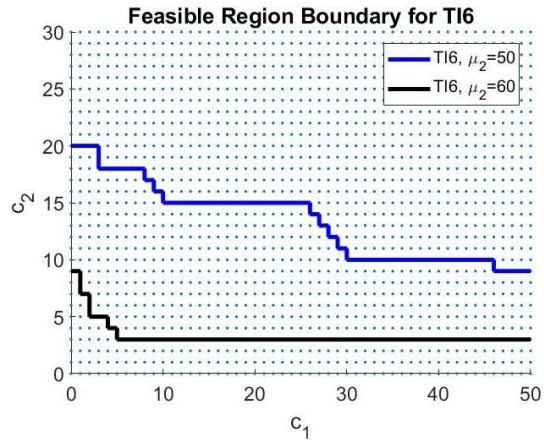
b. Random supply is at node 2
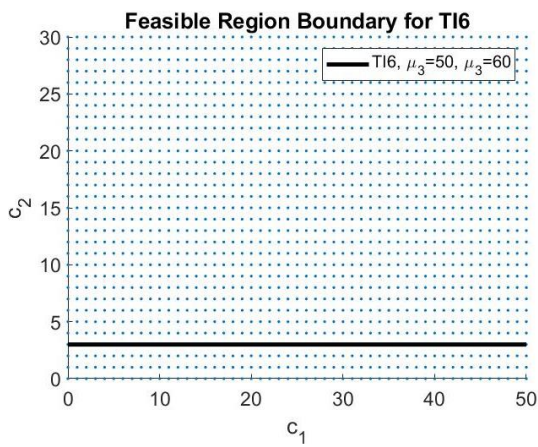
c. Random supply is at node 3
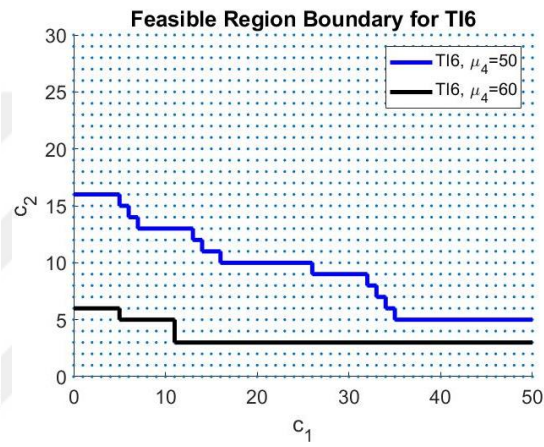
d. Random supply is at node 4

f. Random supply is at node 5

e. Random supply is at node 6

Figure 6.6. Feasible Region Boundaries for Different Locations of Random Supply Node with Means 50 and 60.

After analyzing the effect of changes in supply characteristics, the effect of demand level distributions on the feasible region is studied under $TI7$ as given in Figure 6.7. We employ *d-normal* and *d-uniform* distributions for random demand and generate scenarios accordingly as explained in Chapter 3.1. In this experiment, we run GSA for *d-normal* and *d-uniform* demand level distributions with parameters $(65, 5)$, $(65, 10)$ an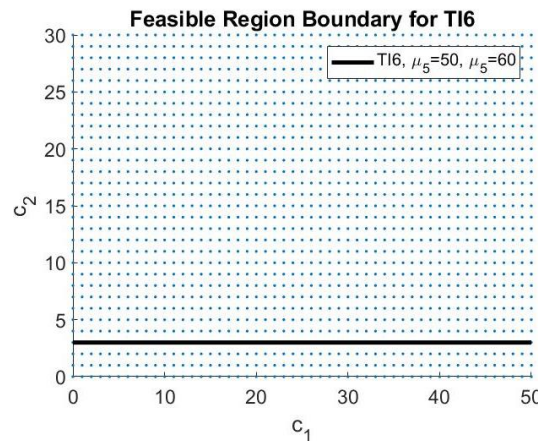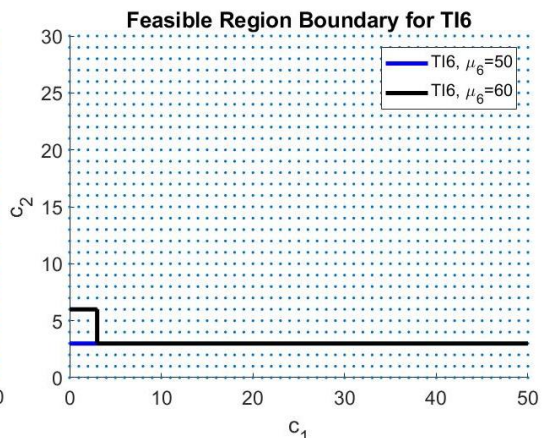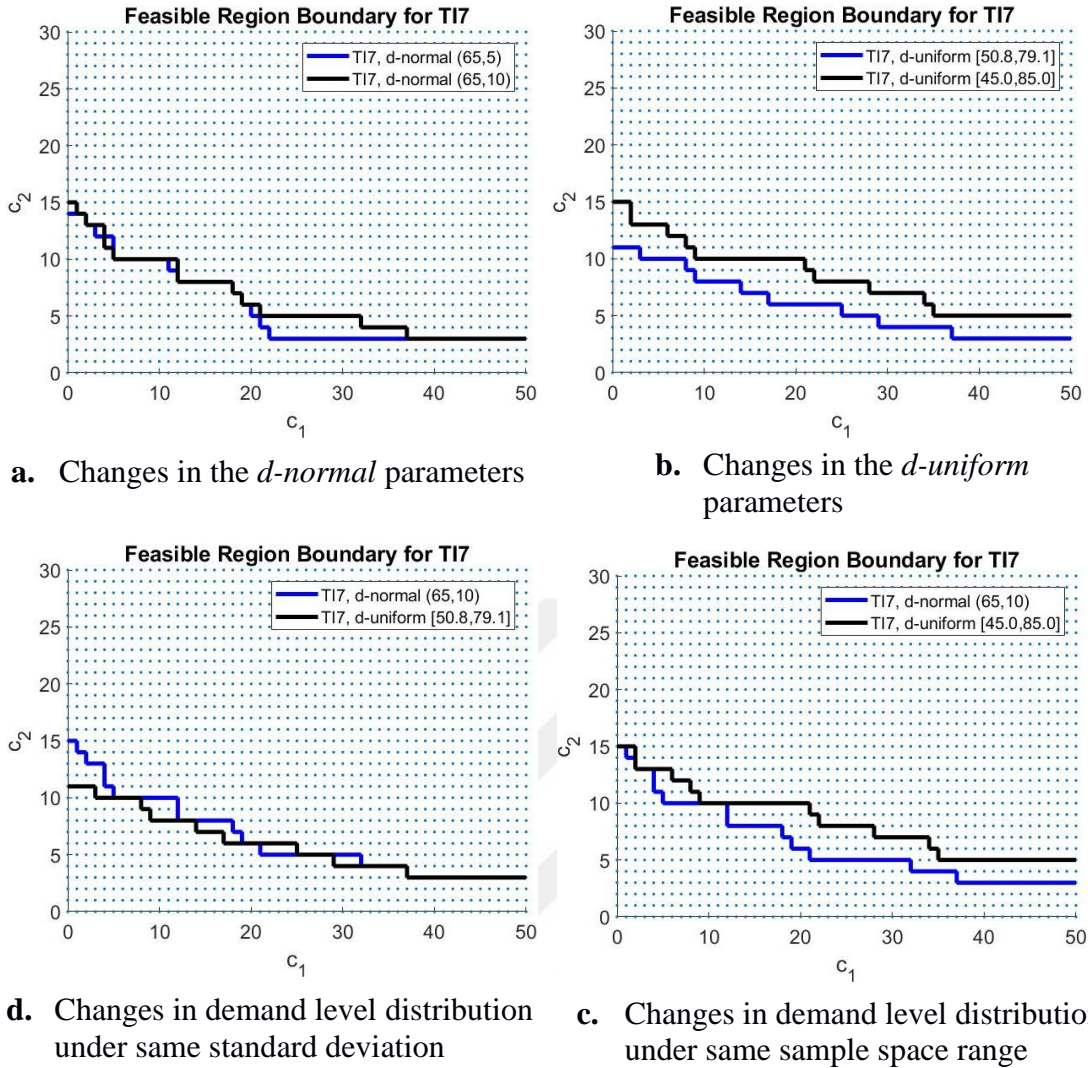d $[50.8, 79.1]$, $[45, 85]$, respectively. The base case parameters are $(65, 10)$ for *d-normal* and $[45, 85]$ for *d-uniform*, where $\mu_j = 65$ and $\sigma_j = 10$ for both of them, and the set of random demand nodes is $\mathcal{D}_R = \{7,8\}$.

First, we test the change in standard deviation using *d-normal* $(65, 5)$ and $(65, 10)$, where the range sample values are $[55, 75]$ and $[45, 85]$, respectively. The range of sample values depends on the standard deviation under the same mean value. Since d-*normal* $(65, 5)$ has a tighter range of sample values than *d-normal* $(65, 10)$, it has lower risk of violating the probabilistic constraint (20), which is $\left(\sum_{\omega \in \Omega_r(c)} q(\omega) \leq \alpha \right)$, as given in Figure 6.7.a. We further test the change in standard deviation using *d-uniform* $[50.8, 79.1]$ and $[45, 85]$. Similarly, we observe that, feasible region shrinks with the increase in standard deviation (see Figure 6.7.b.). Since *d-uniform* $[50.8, 79.1]$ has tighter range of sample values and lower standard variation, which is 10.0, than *d-uniform* $[45,85]$ (standard deviation is 14.14), and hence, it has lower risk of violating (20) compared to *d-uniform* $[45, 85]$, as given in Figure 6.7.b.

Next, we test the change in distribution of demand level under the same mean and standard deviation. In Figure 6.7.c., *d-uniform* $[50.8, 79.1]$ is compared to *d-normal* $(65,10)$, where *d-uniform* $[50.8, 79.1]$ has tighter range of sample values that *d-normal* $(65,10)$ (sample space range is $[45, 85]$). Like in the previous two experiments, feasible region shrinks as the range of sample values enlarges. Finally, in Figure 6.7.d., the effect of the demand level distribution on the same range is tested. Note that, the standard deviation of the *d-uniform* on the range $[45, 85]$ is 14.14, whereas standard deviation of *d-normal* $(65,10)$ is 10. In this case, right tail probabilities of *d-uniform* distribution are larger than *d-normal*, and hence, d-*uniform* has higher risk than *d-normal* under $TI7$.

a. Changes in the *d-normal* parameters

b. Changes in the *d-uniform* parameters

d. Changes in demand level distribution under same standard deviation

c. Changes in demand level distribution under same sample space range

Figure 6.7. Feasible Region Boundaries for Different Demand Level Distributions.

We next conduct a similar experiment by changing the demand mean under the standard deviation. In specific, we compare the cases *d-normal* $(60,10)$ and *d-normal* $(70,10)$ with the base case *d-normal* $(65,10)$. As given in Figure 6.8., we observe that the feasible region shrinks with the increase in mean. Consequently, cost of the optimal capacity expansion increases, see Table 6.7. Note that, optimal cost increases by 10% when demand mean is increased by 5, whereas the increase in cost is 30% if the increase in demand mean is 10. The rate of increase in optimal cost is greater than the rate of increase in demand mean.
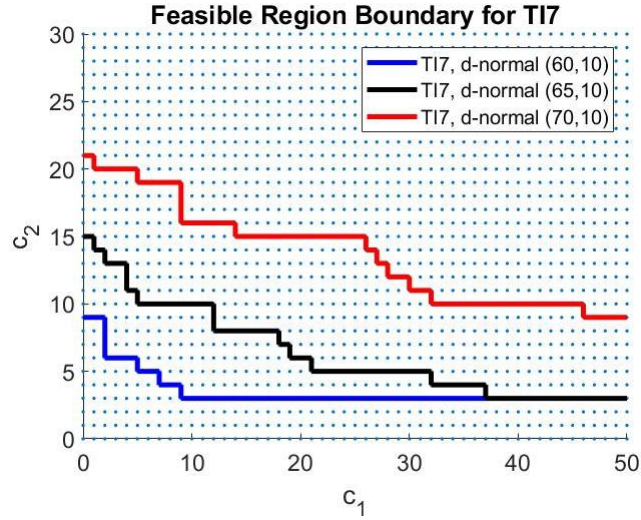
Figure 6.8. Feasible Region Boundaries for Different Demand Level Means.

TABLE 6.7. Optimal Capacity Expansion for $TI7$ under Different Demand Means

(μ, σ)	c^*_{TI7}	$\eta(c^*_{TI7})$	% Increase
$(60, 10)$	[5.0 5.0]	5998.4	–
$(65, 10)$	[5.0 10.0]	6595.9	10%
$(70, 10)$	[9.0 16.0]	7836.9	30%

6.2.4. Effects of Changes in Initial Edge Failure

Scenario generation for initial edge failures (κ) are explained in detail in Chapter 3.2. 10 different set of initially failed edges are selected randomly, and GSA is run 10 times to approximate their feasible regions under $TI1$ and $TI2$. We observe that feasible region resulting from random selection is larger than utilization-based selection in all of the tests. This is an expected outcome, since failures in utilization-based selection are on the edges that are most overloaded, and hence, the failure on these edges increase the "congestion" in the other parts of the network. As a result, risk due to the failures in the most utilized edges are more than the random initial edge failures. Hence, the cost of capacity expansion for utilization-based initial failures is greater than or equal to the capacity expansion cost of random initial failures. It can be said that more investment is required to decrease the impact of targeted failures on the most utilized edges (e.g., terrorist attacks) compared to random failures (e.g., natural disasters). In Table 6.8. below, we give the minimum cost of utilization-based selection and average cost of random selection of the 10 run.

TABLE 6.8. Optimal Capacity Expansion for $TI1$ and $TI2$ under Different Initial Edge Failure Selection

	Initial Edge Failure Selection Method	Initial Failure Probability of Edge i, $i \in \mathcal{E}_{IF}$	$\eta(c^*)$
$TI1$	util. based	0.1	6595.9
$TI1$	random	0.1	5919.8
$TI2$	util. based	0.1	6498.6
$TI2$	random	0.1	5913.3

6.2.5. Effects of Changes in the Parameters of Probabilistic Constraint

In $TI8$ and $TI9$, we experiment the effect of DNS and risk thresholds, ξ and α, respectively. These are the parameters of the probabilistic constraint (20), which is

$\sum_{\omega \in \Omega_r(c)} q(\omega) \leq \alpha$, where $\Omega_r(c) = \{\omega \in \Omega \mid \sum_{\forall j \in \mathcal{D}} \left(1 - y_j^*(\omega, c)\right) L_j(\omega) \geq \xi\}$

and $q(\omega)$ is the probability of the scenario ω.

We first test the change in ξ under the same α. For this test, we set ξ as 0.1, 0.2 and 0.3, where the base case is 0.1. Note that ξ is represented as percentage of the expected total demand, hence $\xi = 0.1$ defines 10% of the total demand ($0.1 \times \sum_{j \in \mathcal{D}} \mu_j$). As given in Figure 6.9.a. feasible region enlarges with the increase in ξ, and hence, the cost of optimal capacity expansion decreases or stays the same, as expected. Next, we run GSA for different values of α under the same ξ. We set α as 0, 0.01 and 0.05, where the base case is 0.05. Similarly, along with the increase in α, feasible region enlarges (see Figure 6.9.b.). Note that, $\alpha = 0$ does not yield any feasible c on the grid under consideration.
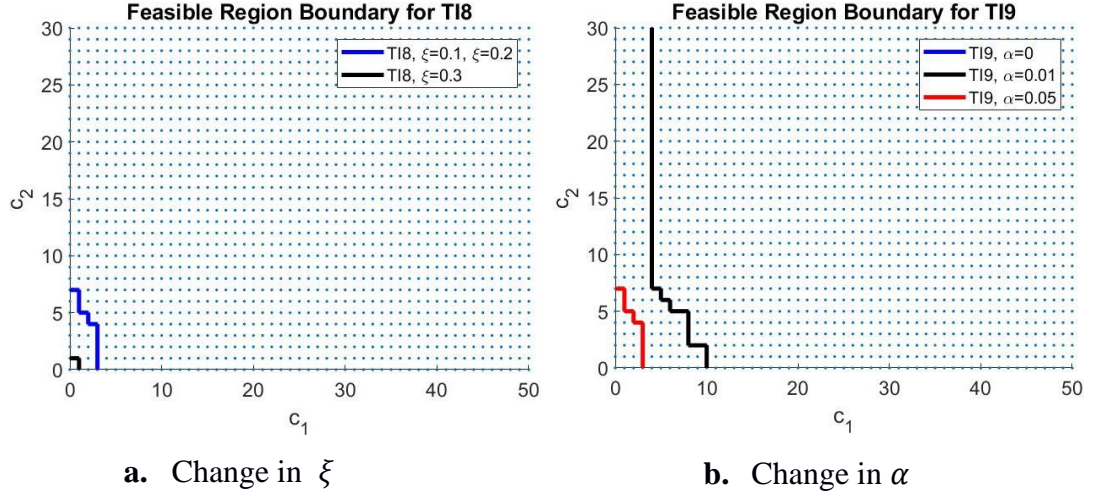
Figure 6.9. Feasible Region Boundaries for Different ξ and α

We further test how the cost of future risk (k_3) changes the optimal solution, and summarize the results in Table 6.9. When cost of future risk ($k_3 = 5000$) is significantly higher than the values of the immediate cost parameters, the optimal solution c^* responds to changes in ξ and α, whereas the optimal cost $\eta(c^*)$ is relatively insensitive. On the other hand, when all the cost components are comparable (when $k_3 = 1000$), both c^* and $\eta(c^*)$ are sensitive to changes in ξ and α. Furthermore, because c_2 has relatively large fixed cost, the solution drives c_2 to 0 at all instances.

TABLE 6.9. Optimal Capacity Expansion for $TI8$ and $TI9$ under Different ξ and α Values

k_3	$\xi^{\dagger}$	α	c^*	$\eta(c^*)$
	10%	0.01	[6.0 5.0]	6034.8
5000	10%	0.05	[4.6 4.1]	5966.6
	30%	0.05	[1.0 0.0]	5900
	10%	0.01	[10.0 0.0]	3250
1000	10%	0.05	[3.0 0.0]	2200
	30%	0.05	[1.0 0.0]	1900

$\dagger$ ξ is represented as percentage of the expected total demand.

As a summary of the numerical study, we investigated and resulted the followings.

i. Effects of Changes in Flow-Network Problem Parameters

Feasible region shrinks with the increase in the cost of unsatisfied demand θ_j under the same ρ_i, whereas feasible region expands with the increase in the cost of overload ρ_i under the same θ_j.

ii. Effects of Changes in Edge Grouping Method

For the test instances that we assign 0.1 as initial failure probability, we find the followings. In eigenvector centrality edge grouping, there is a trade-off between c_1 and c_2, but c_1 is allowed to be 0, since there is only 1 initially failed edge in Group-1. On the other hand, in utilization-based, c_1 must be above a certain level, to compensate the capacity loss experienced due to initially failed Group-1 edges. We observe similar behavior when the initial failure probability is taken as $0.1(ur_i/\Sigma ur_j)$. The main difference is that in this test instance, boundary hits to 0 on both axes in eigenvector centrality edge grouping.

iii. Effects of Changes in Supply and Demand Characteristics

Reduction in random supply mean (while keeping the demand constant) resulted in a narrower feasible region when random supply is located at nodes 1, 2 and 4. We conjecture that this behavior is observed, because, when the random supply generation (cost-less, $\gamma_1 = 0$, in flow network (FP)) is reduced, the other (deterministic) supply nodes have to take up the slack, and may cause "congestion" in other parts of the network, which in turn increases the cascading failure risk. On the other hand, we observe an opposite behavior is observed when the random supply node is 6, and no differences in feasible region boundaries when the same supply means are tested as in nodes 1, 2, 4 and 6. In addition, as random supply is moved between nodes under a certain fixed mean (either 50 or 60), the feasible region boundary also moves.

Increase in random demand sample space (while keeping the supply constant), results in shrinkage in the feasible region. On the other hand, risk increases if we increase the demand standard deviation under the same sample space. In addition, we observe that the feasible region shrinks with the increase in mean, and hence, the cost of the optimal capacity expansion.

iv. Effects of Changes in Initial Edge Failure

We select 10 different set of initially failed edges randomly, and run the GSA. We observe that feasible region resulting from random selection is larger than utilization-

based selection. As a result, more investment is required to decrease the impact of targeted failures on the most utilized edges (e.g., terrorist attacks) compared to random failures (e.g., natural disasters).

v. Effects of Changes in the Parameters of Probabilistic Constraint

Feasible region enlarges with the increase in ξ (while keeping α constant) and hence, the cost of optimal capacity expansion decreases or stays the same, as expected. Likewise, along with the increase in α, feasible region enlarges (see Figure 6.9.b.). Note that, $\alpha = 0$ does not yield any feasible c on the grid under consideration.

CHAPTER 6
CONCLUSIONS AND FUTURE STUDIES

In this study, we introduced a capacity expansion framework to guarantee a certain service level in failure-prone flow-networks. The problem was formulated as a general stochastic optimization model (capacity expansion optimization model) that aims to minimize the total cost of additional edge capacities. Our model allows us to handle different cost structures (linear or non-linear) corresponding to the nature and operation of different systems. We considered a non-linear cost structure that captures both the immediate cost of investment and the cost of future risk. A population-based heuristic algorithm, differential evolution (DE) was employed to compute the cost-optimal additional edge capacities. The constraints of the capacity expansion optimization model are related to the systemic risk measure which composed of two elements: *aggregation function* and *acceptability criterion.* Aggregation function gives us the distribution of total demand-not-satisfied (DNS), and acceptability criterion is the probability of DNS that is above a certain threshold is less than a risk threshold. Hence, feasible region is defined by the additional edge capacities that makes the current system acceptable. To approximate the feasible region, we used a grid search algorithm where the stochastic nature of supply and demand, and initial edge failures are addressed by Monte-Carlo simulations. We performed a series of numerical experiments to understand the effects of system parameters on feasible regions, optimal capacity expansion and their costs using a medium-size general flow-network.

Practitioners from several real-life application areas might benefit from the framework introduced in this study. Both the constraints and the objective function can be defined according to the problem environment. As an example, in a supply chain environment aggregation function can be considered as a system performance indicator and the acceptance criterion might be changed accordingly. Moreover, we can simulate node failures (company) instead of edge failures, and capacity expansion can be defined for

nodes. Similarly, the objective function might be selected among the ones that fit supply-chain context.

The choice flow-network problem parameters depend on the problem environment, and they are selected accordingly. There might be some cases where high amount of penalties applied to unsatisfied demand or edge overloads are not possible. We can adapt our problem to such cases by tuning the cost parameters of the flow-network optimization model. Numerical results show that these parameters directly affect the feasible region, and hence the optimal solution. As a result, it is critical to understand problem environment, and decide on the problem parameters accordingly. We further observe different edge grouping methods result in different feasible regions, consequently, cost-optimal capacity expansion might change. Therefore, selecting a proper edge grouping method that is in line with the nature of real-life application is critical. Another observation is that the location and the capacity of random (cost-less) supply together determine shrinkage or expansion of the feasible region. Thus, both location and capacity of the supply nodes are important factors for achieving the global cost-optimal solution for the entire network. We also test different demand level distributions under the same supply generation capacities. Results reveal that feasible region enlarges along with the tighter range of demand level under the same demand mean. Moreover, feasible region shrinks with the increase in demand mean as expected. Hence, investment cost increase with the increase in demand mean. Finally, we argue that it is critical to decide on cost function parameters, since the balance between the cost of future risk and the value of immediate cost parameters highly affects the optimal solution. When cost of future risk is significantly higher than the values of the immediate cost parameters, the optimal solution responds to changes in the DNS and risk thresholds, whereas the optimal cost is relatively insensitive. On the other hand, when all the cost components are comparable, both the optimal solution and cost are sensitive to changes in the parameters of the probability constraint.

This thesis can be extended in the following research directions: (i) the cost of unsatisfied demand can be directly considered within the objective function. Such an extension would be in line with the real-life practices where cost of shortage in demand satisfaction, e.g., loss of goodwill cost or penalty cost, is included in the cost function. (ii) To control the system operation with more decision variables, the number of edge groups can be increased. One should note that, however, increase in the number of

edge groups would also increase the problem dimension at the price of increased computational complexity. Furthermore, grid search algorithm should also be adapted to the changes in the problem dimension. (iii) Instead of first identifying the feasible region, and then finding the optimal solution, one can solve the problem using an optimization algorithm in a unified framework that handles constraint satisfaction and optimality concurrently. However, this may lead to a poor initial population selection, which is very critical for convergence and optimality in a population-based heuristic algorithm (that performs well for the class of problems considered in this thesis).

REFERENCES

Babayan, A., Kapelan, Z., Savic, D., & Walters, G. (2005). Least-cost design of water distribution networks under demand uncertainty. *Journal of Water Resources Planning and Management*, *131*(5), 375-382.

Baghersad, M., & Zobel, C. W. (2020). Assessing the extended impacts of supply chain disruptions on firms: An empirical study. *International Journal of Production Economics*, 107862.

Baldick, R., Chowdhury, B., Dobson, I., Dong, Z., Gou, B., Hawkins, D., ... & Li, J. (2008, July). Initial review of methods for cascading failure analysis in electric power transmission systems IEEE PES CAMS task force on understanding, prediction, mitigation and restoration of cascading failures. *In 2008 IEEE Power and Energy Society General Meeting-Conversion and Delivery of Electrical Energy in the 21st Century (pp. 1-8)*. IEEE.

Bandt, O. D., & Hartmann, P. (2000). Systemic Risk: A Survey.

Behdani, B., Adhitya, A., Lukszo, Z., & Srinivasan, R. (2012). How to handle disruptions in supply chains–an integrated framework and a review of literature. *Available at SSRN 2114201*.

Biswas, P. P., Suganthan, P. N., Mallipeddi, R., & Amaratunga, G. A. (2019). Optimal reactive power dispatch with uncertainties in load demand and renewable energy sources adopting scenario-based approach. *Applied Soft Computing, 75*, 616-632.

Bonacich, P. (1972). Factoring and weighting approaches to status scores and clique identification. *Journal of mathematical sociology*, *2*(1), 113-120.

Boss, M., Krenn, G., Puhr, C., & Summer, M. (2006). Systemic risk monitor: A model for systemic risk analysis and stress testing of banking systems. *Financial Stability Report*, 11(June), 83-95.

Buldyrev, S. V., Parshani, R., Paul, G., Stanley, H. E., & Havlin, S. (2010). Catastrophic cascade of failures in interdependent networks. *Nature*, *464*(7291), 1025-1028.

Bullard, J., Neely, C. J., & Wheelock, D. C. (2009). Systemic risk and the financial crisis: a primer. *Federal Reserve Bank of St. Louis Review, 91* (September/October 2009).

Capponi, A., & Chen, P. C. (2015). Systemic risk mitigation in financial networks. *Journals of Economic Dynamics and Control*, *58*, 152-166.

Cassidy, A. Feinstein, Z. & Nehorai, A. (2016). Risk measures for power failures in transmission systems. *Chaos*, *26*(11), 113110.

Chakraborty, S. (2015). Generating discrete analogues of continuous probability distributions-A survey of methods and constructions. *Journal of Statistical Distributions and Applications*, *2*(1), 1-30.

Chen, C., Iyengar, G., & Moallemi, C. C. (2013). An axiomatic approach to systemic risk. *Management Science*, *59*(6), 1373-1388.

Cont, R., Moussa, A., Edson, B. S. (2010). Network structure and systemic risk in banking systems. *Network Structure and Systemic Risk in Banking Systems, (December 1, 2010)*.

Crucitti, P., Latora, V., & Marchiori, M. (2004). Model for cascading failures in complex networks. *Physical Review E*, *69*(4), 045104.

Distefano, T., Riccaboni, M., & Marin, G. (2018). Systemic risk in the global water input-output network. *Water resources and economics*, *23*, 28-52.

Eckert, C., & Beer, M. (2019). Measuring Systemic Risk for Mechanical Structures using Conditional Probability.

Eisenberg, L., & Noe, T. H. (2001). Systemic risk in financial systems. *Management Science*, *47*(2), 236-249.

Fang, Y. P., Pedroni, N., & Zio, E. (2014). Comparing network-centric and power flow models for the optimal allocation of link capacities in a cascade-resilient power transmission network. *IEEE Systems Journal*, *11*(3), 1632-1643.

Feinstein, Z., Rudloff, B., & Weber, S. (2017). Measures of systemic risk. *SIAM Journal on Financial Mathematics*, *8*(1), 672-708.

Gantmakher, F. R. (1959). *The theory of matrices* (Vol. 131). American Mathematical Soc.

Ghadge, A., Dani, S., Chester, M., & Kalawsky, R. (2013). A systems approach for modelling supply chain risks. *Supply chain management: an international journal*.

Govindan, K., Fattahi, M., & Keyvanshokooh, E. (2017). Supply chain network design under uncertainty: A comprehensive review and future research directions. *European Journal of Operational Research*, *263*(1), 108-141.

Hinojosa, Y., Puerto, J., & Saldanha-da-Gama, F. (2014). A two-stage stochastic transportation problem with fixed handling costs and a priori selection of the distribution channels. *Top*, *22*(3), 1123-1147.

Kaufman, G. G., & Scott, K. E. (2003). What is systemic risk, and do bank regulators retard or contribute to it?. *The Independent Review*, *7*(3), 371-391.

Kamalahmadi, M., & Parast, M. M. (2017). An assessment of supply chain disruption mitigation strategies. *International Journal of Production Economics, 184*, 210-230.

Kinney, R., Crucitti, P., Albert, R., & Latora, V. (2005). Modeling cascading failures in the North American power grid. *The European Physical Journal B-Condensed Matter and Complex Systems*, *46*(1), 101-107.

Kleindorfer, P. R., & Saad, G. H. (2005). Managing disruption risks in supply chains. *Production and operations management*, *14*(1), 53-68.

Korkali, M., Veneman, J. G., Tivnan, B. F., Bagrow, J. P., & Hines, P. D. (2017). Reducing cascading failure risk by increasing infrastructure network interdependence. *Scientific reports*, *7*, 44499.

La, R. J. (2017). Cascading failures in interdependent systems: Impact of degree variability and dependence. *IEEE Transactions on Network Science and Engineering*, *5*(2), 127-140.

Ledwoch, A., Brintrup, B., Mehnen, J. & Tiwari, A. (2016). Systemic risk assessment in complex supply networks. *IEEE Systems Journal*, *12*(2), 1826-1837.

Li, Y., & Zobel, C. W. (2020). Exploring supply chain network resilience in the presence of the ripple effect. *International Journal of Production Economics*, 107693.

Lucas, K., Renn, O., Jaeger, C., & Yang, S. (2018). Systemic risks: a homomorphic approach on the basis of complexity science. *International Journal of Disaster Risk Science*, *9*(3), 292-305.

MATLAB. (2016). *version 9.1.0. 441655 (R2016b)*. Natick, Massachusetts: The MathWorks Inc.

Mallipeddi, R., Suganthan, P. N., Pan, Q. K., & Tasgetiren, M. F. (2011). Differential evolution algorithm with ensemble of parameters and mutation strategies. *Applied soft computing*, *11*(2), 1679-1696.

Oehmen, J., Ziegenbein, A., Alard, R., & Schönsleben, P. (2009). System-oriented supply chain risk management. *Production planning and control*, *20*(4), 343-361.

Olson, D. L. & Swenseth, S. R. (2014). Trade-offs in supply chain system risk mitigation. *Systems Research and Behavioral Science*, *31*(4), 565-579.

Pitilakis, K., Argyroudis, S., Kakderi, K., & Selva, J. (2016). Systemic vulnerability and risk assessment of transportation systems under natural hazards towards more resilient and robust infrastructures. *Transportation research procedia*, *14*, 1335-1344.

Poudel, S., Dubey, A., & Bose, A. (2019). Risk-Based Probabilistic Quantification of Power Distribution System Operational Resilience. *IEEE Systems Journal*.

Qiu, R., & Wang, Y. (2016). Supply chain network design under demand uncertainty and supply disruptions: a distributionally robust optimization approach. *Scientific Programming*, 2016.

Santoso, T., Ahmed, S., Goetschalckx, M., & Shapiro, A. (2005). A stochastic programming approach for supply chain network design under uncertainty. *European Journal of Operational Research*, *167*(1), 96-115.

Salomon, J., Broggi, M., Kruse, S., Weber, S., & Beer, M. (2020). Resilience Decision-Making for Complex Systems. *ASCE-ASME J Risk and Uncert in Engrg Sys Part B Mech Engrg, 6*(2).

Scheibe, K. P., & Blackhurst, J. (2018). Supply chain disruption propagation: a systemic risk and normal accident theory perspective. *International Journal of Production Research*, *56*(1-2), 43-59.

Schmitt, A. J., & Singh, M. (2012). A quantitative analysis of disruption risk in a multi-echelon supply chain. *International Journal of Production Economics*, *139*(1), 22-32.

Stecke, K. E., & Kumar, S. (2009). Sources of supply chain disruptions, factors that breed vulnerability, and mitigating strategies. *Journal of Marketing Channels*, *16*(3), 193-226.

Storn, R. (1996, June). On the usage of differential evolution for function optimization. In *Proceedings of North American Fuzzy Information Processing* (pp. 519-523). IEEE.

Storn, R., & Price, K. (1997). Differential evolution–a simple and efficient heuristic for global optimization over continuous spaces. *Journal of global optimization*, *11*(4), 341-359.

Świerczek, A. (2014). The impact of supply chain integration on the "snowball effect" in the transmission of disruptions: An empirical evaluation of the model. *International Journal of Production Economics*, *157*, 89-104.

Sun, X., Liu, C., Chen, X., & Li, J. (2017). Modeling systemic risk of crude oil imports: Case of China's global oil supply chain. *Energy*, *121*, 449-465.

Tang, L., Jing, K., He, J., & Stanley, H. E. (2016). Complex interdependent supply chain networks: Cascading failure and robustness. *Physica A: Statistical Mechanics and its Applications*, *443*, 58-69.

Upper, C., & Worms, A. (2004). Estimating bilateral exposures in the German interbank market: Is there a danger of contagion?. *European economic review*, *48*(4), 827-849.

Watts, D. J. (2002). A simple model of global cascades on random networks. *Proceedings of the National Academy of Sciences, 99*(9), 5766-5771.

Wynne, B., & Dressel, K. (2010). Cultures of uncertainty–transboundary risks and BSE in Europe. *In Transboundary risk management* (pp. 135-168). Routledge.

Zhang, J., & Moura, J. M. (2017). Cascading edge failures: A dynamic network process. *IEEE Transactions on Network Science and Engineering*, *5*(4), 288-300.

Zhao, Z., Zhang, P., & Yang, H. (2015). Cascading failures in interconnected networks with dynamical redistribution of loads. *Physica A: Statistical Mechanics and its Applications*, *433*, 204-210.

Zhao, K., Scheibe, K., Blackhurst, J., & Kumar, A. (2018). Supply chain network robustness against disruptions: Topological analysis, measurement, and optimization. *IEEE Transactions on Engineering Management*, *66*(1), 127-1

APPENDIX 1 – EDGE CAPACITIES

Table A1.1. Edge Capacities

i	$\bar{P}_i$	i	$\bar{P}_i$	i	$\bar{P}_i$	i	$\bar{P}_i$
1	$1e+05$	13	50	25	50	37	45
2	$1e+05$	14	50	26	55	38	45
3	$1e+05$	15	50	27	50	39	45
4	$1e+05$	16	50	28	50	40	45
5	$1e+05$	17	50	29	50	41	45
6	$1e+05$	18	55	30	50	42	45
7	$1e+05$	19	50	31	50	43	45
8	$1e+05$	20	50	32	50	44	45
9	$1e+05$	21	50	33	50	45	45
10	$1e+05$	22	50	34	45	46	45
11	$1e+05$	23	50	35	45		
12	$1e+05$	24	50	36	45		

APPENDIX 2 – EDGE GROUP ASSIGNMENTS

Group assignments are detailed in the following table. Threshold for Group-1 is 0.1 for eigenvector centrality based edge grouping ($TI1$) and is 0.4 for utilization-based grouping ($TI2$ and $TI3$). Since, supply and demand edges are introduced for modeling purposes, we don't show their group assignments.

Table A2.1. Edge Group Assignments

TI1				TI2				TI3			
Group-1		Group-2		Group-1		Group-2		Group-1		Group-2	
ζ_{iD}	i	ζ_{iD}	i	ur_i	i	ur_i	i	ur_i	i	ur_i	i
0.34	13	0.09	38	0.78	23	0.37	42	0.80	23	0.39	39
0.34	14	0.08	24	0.78	18	0.37	28	0.79	18	0.36	41
0.33	16	0.08	37	0.77	17	0.37	32	0.75	17	0.35	27
0.33	33	0.08	45	0.74	45	0.36	27	0.73	45	0.32	42
0.33	17	0.08	31	0.67	35	0.31	14	0.68	35	0.28	14
0.33	15	0.08	29	0.62	26	0.30	15	0.64	34	0.27	19
0.13	30	0.07	23	0.61	20	0.24	21	0.64	26	0.27	21
0.13	34	0.06	27	0.56	30	0.24	19	0.63	30	0.25	15
0.13	32	0.06	44	0.56	34	0.22	22	0.59	20	0.20	22
0.12	28	0.05	46	0.54	16	0.12	25	0.58	28	0.17	33
0.11	40	0.03	43	0.48	40	0.07	38	0.43	36	0.11	25
0.11	42	0.02	26	0.46	13	0.07	37	0.43	16	0.10	38
0.10	39	0.01	21	0.44	36	0.07	29	0.43	40	0.10	29
0.10	41	0.005	22	0.44	39	0.07	31	0.42	13	0.10	31
		0.08	35	0.41	41	0.04	44	0.41	32	0.09	37
		0.01	19			0.02	24			0.04	24
		0.01	36			0.00	33			0.04	44
		0.01	25			0.00	46			0.01	43
		0.01	20			0.00	43			0.00	46
		0.06	18								